

THE HYPERLOOP: A TOP-DOWN SYSTEMS
ENGINEERING EVALUATION OF THE
TECHNICAL AND ECONOMIC FEASIBILITY

BROOKS HALLIN, '14

SUBMITTED TO THE
DEPARTMENT OF MECHANICAL AND AEROSPACE ENGINEERING
PRINCETON UNIVERSITY
IN PARTIAL FULFILLMENT OF THE REQUIREMENTS OF
UNDERGRADUATE INDEPENDENT WORK.

FINAL REPORT

MAY 1, 2014

PROFESSOR NOSENCHUCK
PROFESSOR HULTMARK
MAE 442
160 PAGES
FILE COPY

© Copyright by Brooks Hallin, 2014.
All Rights Reserved

This thesis represents my own work in accordance with University regulations.

Abstract

Elon Musk captured the world’s attention in August 2013 when he released a high-level alpha design for a fifth mode of transportation called the Hyperloop—a reduced-pressure tube that contains pressurized capsules driven within the tube by a number of linear electric motors. His proposal was motivated by the proposed high speed rail system between Los Angeles and San Francisco that would cost \$68.4 billion and have a total trip time of 2 hours and 38 minutes, providing limited transportation improvements. The alpha design outlines a passenger system between the same two cities that could be built for only \$6 billion and have a faster travel time of only 35 minutes, offering significant advancements.

While this alpha document provided a complete overview with clear goals for the system, more thorough engineering analysis was required to assess its technical viability as well as its economical reality. Each subsystem was broken down into its fundamental parameters and governing physical principles. These were then analyzed to evaluate their effect on both their corresponding subsystem and the overall Hyperloop performance. Several modifications were suggested to make the system feasible. Issues downplayed by the alpha document were brought to attention and their impacts were discussed. Economics, politics, and other human factors were also considered to complement the engineering analysis to gain a top-level perspective on this new mode of transportation. From the analysis it was determined that the Hyperloop could make the journey in 36.35 minutes with a revised capital expenditure of \$16.84 billion. The Hyperloop would be recommended as an alternative to the high speed rail and has the potential to revolutionize transportation across the world.

Acknowledgements

I would like to thank my adviser, Professor Nosenchuck, for all his support, wisdom, time, and energy throughout the senior thesis. It was rewarding working with someone with so much experience and knowledge as I was encouraged to explore areas of engineering I would have never before considered.

In addition, without the guidance and teaching from the entire Mechanical and Aerospace Department faculty and staff I would have never developed the tool set to take on such a complex project that reaches across all disciplines of the department.

To my family for all their love and support.

Contents

Abstract	iii
Acknowledgements	iv
List of Tables	x
List of Figures	xi
List of Symbols	xv
1 Introduction	1
1.1 Background and Significance	1
1.1.1 Motivation Behind Elon Musk’s Proposal	1
1.1.2 Seeking an Alternative to High Speed Rail	2
1.1.3 Similar Proposals to the Hyperloop	3
1.2 Objectives	5
2 System Overview	6
2.1 Technical Components and Principles	6
2.1.1 Aerodynamic Drag	6
2.1.2 Capsule Propulsion System	7
2.1.3 Capsule Suspension System	8
2.1.4 Vacuum Pumps	9
2.1.5 Compressor	9
2.1.6 Hyperloop Route	10
2.1.7 Infrastructure	10
2.2 Total Cost Overview	11
2.2.1 Estimated Capsule Cost and Weight	11
2.2.2 Total System Capital Costs	11
3 Aerodynamic Analysis of the Hyperloop	14
3.1 Overview	14
3.2 Introduction	14

3.3	General Flow Analysis	15
3.4	Aerodynamic Drag Model	16
3.4.1	F_1 Derivation	17
3.4.2	F_2 Derivation	18
3.4.3	F_3 Derivation	19
3.5	Numerical Analysis	20
3.6	External Studies	23
3.7	Summary	26
4	Propulsion Technology for the Hyperloop	28
4.1	Introduction	28
4.2	The Linear Induction Motor (LIM)	28
4.2.1	Background	28
4.2.2	Hyperloop Alpha Propulsion Design	30
4.3	Propulsion Analysis	31
4.3.1	Propulsion Times and g -force Analysis	32
4.3.2	Propulsion Work and Power	33
4.3.3	Regenerative Braking	35
4.3.4	Propulsion Costs	37
5	Air Bearing Suspension System	40
5.1	Introduction	40
5.2	Alpha Design	40
5.3	Suspension Gap Flow Characteristics	42
5.3.1	Gap Temperature	42
5.3.2	Knudsen Number and Flow Characterization	42
5.3.3	Couette Flow	43
5.3.4	Lubrication Theory	45
5.3.5	Suspension Lift and Required Compressor Air Input	49
5.3.6	Control Overview	50
5.4	Maglev Cost Analysis: An Alternative Suspension Option	54
6	In-Depth Analysis of the Quarter Car Suspension System using H_∞ Control Synthesis	58
6.1	Introduction	58
6.2	Quarter Car Suspension Model	59
6.3	Hydraulic Actuator Model	61

6.4	Preliminary Analysis	62
6.5	H_∞ Control Synthesis	64
6.6	Robust μ Synthesis	69
6.7	Other Papers/Other Control Methods	72
6.8	Summary	72
7	Vacuum Pump Technology for the Hyperloop	73
7.1	Introduction	73
7.2	Analysis for Tube Vacuumization Time	73
7.2.1	Orifice Conductance	73
7.2.2	Long Pipe Conductance	74
7.2.3	Vacuumizing Time	74
7.3	Numerical Analysis of the Vacuum Pump	75
7.3.1	Initial Pump-Down from Atmospheric Conditions to Target Tube Pressure	75
7.3.2	Airlock Chamber Evacuation	79
7.3.3	Power Requirements	80
7.4	Available Vacuum Pumps, Additional Influencing Factors, and Rec- ommendations	80
7.5	Summary	85
8	Hyperloop Compressor	86
8.1	Introduction	86
8.2	Alpha Compressor Design	86
8.3	Diffuser Compressor Design	87
8.4	Intercoolers: Water Coolant Mass Flow Rate	89
8.5	Summary	91
9	Modeling the Hyperloop Route	92
9.1	Introduction	92
9.2	Route Visualization	93
9.2.1	Capsule Deceleration	93
9.2.2	Preliminary Bend Radii Analysis	94
9.2.3	Route Journey: Speed and Position as Functions of Time since Departure	96
9.2.4	Departure Separation, Passengers, and Number of Capsules	99
9.3	Track Bend Radius: In-Depth Look	103

9.4	Summary	108
10	Hyperloop Infrastructure	109
10.1	Tube Route Layout Schemes	109
10.2	Tube Material and Structure	110
10.3	Tube Thickness Numerical Analysis	110
10.4	Pylons, Expansion Joints, and Dampers	112
10.5	Large-Scale Engineering and Infrastructure Projects	113
10.5.1	Princeton Plasma Physics Laboratory and Engineering Costs .	113
10.5.2	Other Large-Scale Infrastructure Project Costs	115
10.6	Hyperloop Infrastructure Costs	116
10.6.1	Tube Costs	116
10.6.2	Pylon Construction Costs	116
10.6.3	Tunneling Costs	118
10.7	Total Civil Infrastructure Costs Summary	119
11	Effect of Changing System Parameters on Overall Trip Time and System Costs	120
11.1	Introduction	120
11.2	Effect of Changing Tube Diameter	120
11.3	Effect of Changing Capsule Length	124
11.4	Effect of Changing Tube Pressure	126
11.5	Effect of Changing Suspension Gap Height	129
11.6	Other effects	130
11.7	Total Costs	130
12	Conclusion	133
A	Important System Parameters	143

List of Tables

2.1	Estimated capsule cost and mass breakdown.	11
2.2	Estimated total cost of Hyperloop passenger transportation system. .	12
2.3	Estimated total cost of Hyperloop passenger plus vehicle transportation system.	13
4.1	Hyperloop propulsion: g -force, minimum track length, alpha times, and minimum times.	33
4.2	Hyperloop propulsion work and power requirements for $1g$ acceleration.	35
4.3	Hyperloop regenerative braking energy recovery vs. propulsion energy.	37
4.4	Hyperloop Propulsion Components Capital Costs Per Station - Tube Side.	38
5.1	Air suspension system parameters	41
5.2	Max Couette shear stress in suspension gap.	45
5.3	Maglev guideway cost assessment extrapolated to Hyperloop route . .	57
6.1	Hyperloop Parameters for Quarter Car Suspension Model	61
6.2	H_∞ Norm for Various β Conditions	66
7.1	Parameters for Determining Orifice Conductance	75
9.1	Minimum bend radius for $0.5g$ lateral acceleration.	96
9.2	Alpha route segment times and distances traveled since leaving L.A. .	96
9.3	Departure delays and minimum deceleration rates	99
11.1	Total Capital Cost Comparison	130

List of Figures

1.1	Energy Cost Per Passenger for Various Modes of Transportation . . .	3
2.1	Hyperloop Capsule Concept Sketch	8
3.1	Aerodynamic Model Schematic of Hyperloop	16
3.2	Aerodynamic Model: F3 Derivation	20
3.3	Aerodynamic Drag as Function of Tube Pressure and Capsule Velocity	21
3.4	Aerodynamic Drag: Pressure Ranges Between 0 and 600 Pa	22
3.5	Aerodynamic Drag vs. Tube Pressure for Alpha Document Conditions	22
3.6	Aerodynamic Drag vs. Blockage Ratio	23
3.7	Ansys Hyperloop CFD: Wall Shear Stress	25
3.8	Ansys Hyperloop CFD: Flow Velocity Contours	26
4.1	Hyperloop Propulsion: Double-Sided Linear Induction Motor (DSLIM) Schematic	29
4.2	Hyperloop Propulsion: Rotor and Stator Configuration	31
4.3	Propulsion: Regenerative Braking Power	36
4.4	Propulsion: Regenerative Braking Energy Recovered	37
5.1	Alpha Air Bearing Suspension Desgin	41
5.2	Suspension Gap: Coutte Velocity Profile - h_{min}	44
5.3	Suspension Gap: Coutte Velocity Profile - h_{max}	44
5.4	Lubrication theory schematic and force diagram.	46
5.5	Suspension Gap: Journal Bearing Analysis - h_{min}	48
5.6	Suspension Gap: Journal Bearing Analysis - h_{max}	48
5.7	Suspension Ski Control Volume	49
5.8	Air Suspension Control: Uncontrolled Response to Bump	51
5.9	Suspension Control: Permissible Incoming Bump vs. Time Since Initial Bump Encounterd	52

5.10	Suspension Control: Permissible Incoming Bump vs. Distance Since Initial Bump Encountered	53
5.11	Human Movement: Vertical Displacement of Capsule Center of Mass	54
5.12	Capital Construction Costs for California-Nevada Interstate Maglev Project	56
6.1	Quarter Car Suspension Model	59
6.2	Suspension Control: Hydraulic Actuator	62
6.3	Bode Plot Showing the Tire Hop and Rattlespace Frequencies	63
6.4	H_∞ model for Quarter Car Suspension System	64
6.5	Target Closed-Loop Response vs. Open-Loop Response	65
6.6	Closed-loop for H_∞ synthesized controllers for each blending parameter, β , compared to passive suspension system (open-loop)	67
6.7	Time Response for Road Disturbance Signal: Effect of Blending Parameter, β	68
6.8	Time Response for Road Disturbance Signal: Robust μ Synthesized Controller vs. Open-Loop.	69
6.9	Time Response for Road Disturbance Signal: H_∞ Nominal Controller and Model Uncertainty	70
6.10	Time Response for Road Disturbance Signal: μ Synthesized Robust Controller and Model Uncertainty	71
7.1	Schematic of Hyperloop Tube Section to be Vacuumized	75
7.2	Available Vacuumizing Speed vs. Tube Diameter	76
7.3	Vacuum Pump-Down Time vs. Tube Pressure	77
7.4	Vacuum Pump-Down Time vs. Tube Pressure: Pressure Range 0 to 200 Pa	78
7.5	Airlock Pump-Down Time vs. Target Pressure	79
7.6	Rotary Vane Backing Pump	81
7.7	Roots Vacuum Pump	82
7.8	Pfeiffer CombiLine 1902	83
7.9	Rotary Pump Motor Power vs. Intake Pressure	84
8.1	Alpha Compressor Schematic	87
9.1	Effect of Aerodynamic Drag on Hyperloop Position	93
9.2	Effect of Aerodynamic Drag on Hyperloop Speed	94
9.3	Aerodynamic Drag Force vs. Time	95

9.4	Power Loss Due to Aerodynamic Drag	95
9.5	Speed of Hyperloop Capsule vs. Time from L.A. Departure	98
9.6	Position of Hyperloop Capsule vs. Time from L.A. Departure	98
9.7	Departure Delay and Minimum Deceleration	100
9.8	Passengers per Hour vs. Departure Delay	102
9.9	Number of Capsules vs. Departure Delay	102
9.10	Lateral Acceleration vs. Time from L.A. Departure	104
9.11	Example Route Section with Corresponding Bend Radii	105
9.12	Route Smoothing Options and Required Land Area	105
9.13	San Francisco Suburban Area Where Route Path Needs to Be Altered	106
9.14	Suburban Route Smoothing and Infrastructure Displacement	107
10.1	Tube Construction Costs vs. Tube Diameter	117
10.2	Total Civil Infrastructure Capital Costs	119
11.1	Total Trip Time vs. Blockage Ratio	121
11.2	Total Trip Time vs. Tube Diameter	122
11.3	Propulsion Energy vs. Tube Diameter	123
11.4	Total Trip Time vs. Capsule Length	124
11.5	Propulsion Energy vs. Capsule Length	125
11.6	Capsule Capital Costs vs. Capsule Length	126
11.7	Total Trip Time vs. Tube Pressure	127
11.8	Total Trip Time vs. Tube Pressure: 0 - 500 Pa	127
11.9	Propulsion Energy vs. Tube Pressure	128
11.10	Total Trip Time vs. Gap Height	129
11.11	Capital Cost Comparison: Alpha vs. Revised	131

List of Symbols

v_c	Speed of Sound	15
γ	Ratio of Specific Heats	15
R	Specific Gas Constant	15
T	Temperature	15
u_e	Fluid Flow Velocity	15
M	Mach Number	15
Re	Reynolds Number	15
μ	Dynamic Viscosity	15
D_{tube}	Diameter of Hyperloop Tube	16
h_{gap}	Suspension Gap Height	16
$W_{capsule}$	Width of Capsule	16
$H_{capsule}$	Height of Capsule	16
$L_{capsule}$	Length of Capsule	16
b_r	Blockage Ratio	16
SA	Capsule Frontal Surface Area	16
SA_0	Tube Cross-Sectional Area	16
F	Force	17
τ	Shear Stress	19
p	Pressure	19
g_{force}	g -force	32
t	Time	32
m_c	Mass of Capsule	33
W	Work	33
P	Power	33
η	Efficiency	34
W_{ski}	Air Suspension Ski Width	41
L_{ski}	Air Suspension Ski Height	41
N_{ski}	Number of Air Suspension Skis	41

α	Ski Angle of Attack	41
V	Volume	42
Kn	Knudsen Number	43
C	Conductance	74
M	Molar Mass	74
S_e	Available Vacuumizing Speed	74
S_0	Nominal Vacuumizing Speed	74
r	Compression Ratio	88
r_p	Pressure Ratio	88
\dot{m}	Mass Flow Rate	88
c_p	Ratio of Specific Heats at Constant Pressure	88
\dot{Q}	Heat Transfer Rate	89
r_{min}	Minimum Radius of Curvature	94
σ	Normal Stress	111

Chapter 1

Introduction

1.1 Background and Significance

1.1.1 Motivation Behind Elon Musk's Proposal

Elon Musk captured the world's attention in August 2013 when he released a high-level alpha design for a fifth mode of transportation called the Hyperloop—a reduced pressure tube that contains pressurized capsules driven within the tube by a number of linear electric motors. His proposal was motivated by California's proposed “high speed” rail system between Los Angeles and San Francisco that would cost \$68.4 billion, have a travel time of 2 hours 38 minutes, a \$105 one-way ticket price, and high energy costs [34]. Disappointed, Musk established the following objectives for the Hyperloop:

- Lower cost
- Faster
- Safer
- More convenient
- Immune to weather
- Sustainably self-powering/Environmentally friendly
- Resistant to earthquakes
- Not disruptive to those along the route

The alpha design outlines a passenger system between the same two cities that could be built for only \$6 billion, achieve a faster travel time of only 35 min, have cheaper tickets of \$20, and remove human control error and unpredictable weather from the system, while managing to satisfy every other objective on this list. The Hyperloop seeks to revolutionize transportation, but major questions remain about the possibility of actually building this system and meeting these objectives.

1.1.2 Seeking an Alternative to High Speed Rail

Any transportation system connecting two major cities such as L.A. and San Francisco will require a massive investment that will need to be met with returns exceeding expectations. California’s “high speed” rail system does not seem to warrant this investment. The proposed rail would be one of the most expensive per kilometer and slowest in the world. It is not only more expensive to operate than planes if unsubsidized, but also slower and less safe than flying by two orders of magnitude (based on estimates from the Bureau of Transportation Statistics [59]). The returns of the proposed high speed rail are minimal when it does not reduce current trip times or reduce the cost relative to existing modes of transportation. The Hyperloop offers a promising alternative.

There are several environmental advantages of the Hyperloop. A preliminary energy cost analysis presented in the alpha document (Figure 1.1) further reveals substantially higher costs for the high speed rail compared to that of proposed Hyperloop. In addition, trains require wide sloths of land and are also loud, require fences, can be safety hazards to others, and have a higher risk of derailment. The noise level of the Hyperloop will be virtually silent compared to the damaging noise levels of trains and the Hyperloop will produce negligible ground vibration. Furthermore, there is no legislation to prevent the Hyperloop’s implementation and the California environmental laws that will ramp up in 2020 will greatly favor this new mode of transportation. In January 2014, Nick Garzilli submitted a request to place the Transportation Innovation Act on the California ballot. This act would suspend further issuance of bonds and construction of the high speed rail system in order to allow for the construction and operation of innovative technologies that are faster and more reliable, energy efficient, flexible, and less expensive [20].

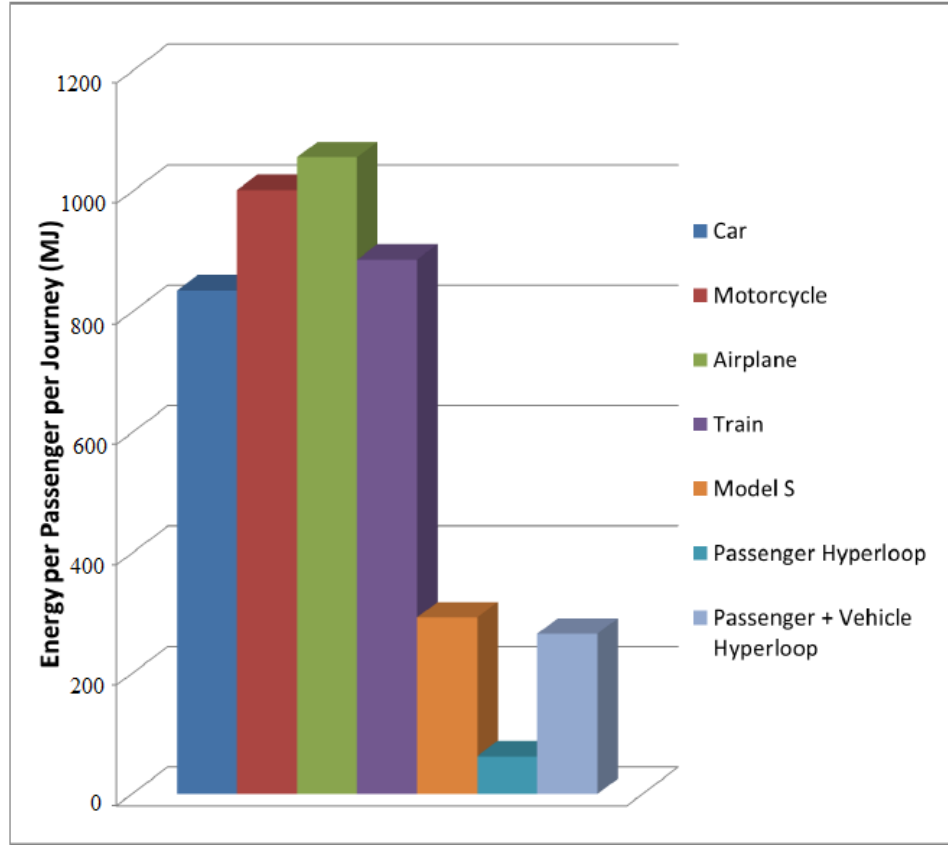


Figure 1.1: Energy cost per passenger for a journey between Los Angeles and San Francisco for various modes of transport [34].

The Hyperloop may not be the right solution for all travel distances. Musk discusses an inflection point where for high traffic city pairs less than 1500 km apart the Hyperloop is the right solution, but for greater distances hypersonic air travel makes more sense.

1.1.3 Similar Proposals to the Hyperloop

Prior to Musk’s Hyperloop proposal, Robert Goddard, Rand Corporation, and ET3 have presented similar ideas. Many use the term evacuated tube transportation (ETT) to describe this transportation technology.

Robert Goddard, the revolutionary rocket scientist, first conceptualized vac-trains in the 1910s. These trains would levitate via magnets and move along a partial vacuum tube at very high speeds due to lack of air resistance [19].

In 1972, Rand Corporation published a paper proposing the Very High Speed Transit System (VHSTS), a maglev-based underground vacuum tunnel system [48].

A main line would run diagonally across the country and could make the trip between New York and L.A. in only 21 minutes while achieving unrealistic speeds of 14,000 mph.

Daryl Oster formed the company Evacuated Tube Transport Technologies (ET3) to pursue his idea for an ETT system with the claim of transporting passengers between New York and L.A. in only 45 minutes, and ultimately sending passengers and cargo from New York to Beijing in 2 hours [38]. Like Musk, Oster was dissatisfied with current transportation dependencies and has called for a new paradigm shift in transportation. Transportation has the potential to be the biggest growth market in the world and his global vision would connect the world with a network of evacuated tubes within the next 20 years. He first conceived the idea in the 1980s and later received his first patent in 1999. The initial designs would transport 6 passengers or 367 kg of cargo in a system of vacuum tubes at speeds of 600 km/hr, but eventually be propelled via maglev up to 6,500 km/hr (Mach 5) in straight unpopulated areas. This really embodies ET3 trademarked phrase “Space Travel on Earth” as this hypothetical top speed nearly doubles the fastest recorded airspeed record. While Oster’s proposed \$10 – \$20 trillion investment to displace 90% of the world’s current transportation scheme is extraordinarily ambitious and unrealistic, the company is currently focusing on finding 5 km stretches of land to test the elements of their concept needed to achieve 600 km/hr. ET3 has estimated this test track will cost \$20 million, but upon large-scale implementation the costs will drop to \$1.86 million per km. Oster has also claimed to be able to build his system between L.A. and San Francisco for 1/10 the cost of the proposed high speed rail as well as 1/50 the energy. The ET3 website has a table comparing ET3 costs with high speed rail costs [37]. However, neither Oster nor the other 244 contributing ET3 licensees have released any design plans or detailed cost estimates to back these claims.

The Rand and ET3 designs are centered around drawing hard or near hard vacuum in the tube and using electromagnetic suspension. This is problematic as it is very difficult to maintain the vacuum they seek. An alternative is to have a low pressure system set to a level where standard commercial pumps can easily overcome an air leak and the transport capsules can handle variable air density. This system would be inherently robust. To avoid the high costs of maglev suspension technology, an air suspension system could be implemented. Modifications to these earlier ideas, provide the basis for the Hyperloop concept as a new method of public transit.

1.2 Objectives

This thesis aims to provide a detailed analysis of the Hyperloop defined by Elon Musk's alpha document. The existing literature was surveyed to gain insight into the individual subsystems of the Hyperloop. While the literature is replete with interest, many engage in hand waving without justification. More detailed engineering analysis was necessary to determine the technical viability of this system. The objective was to then individually break down each subsystem and to develop performance and cost metrics to bring all the elements together. These metrics could then be used to compare to other transportation systems. Complexities of the design were simplified when necessary and modifications were suggested to make the concept realizable. Economics, politics, and other human factors were also considered to complement the engineering analysis to gain a top-level perspective on this new mode of transportation.

Chapter 2

System Overview

The Hyperloop is a single system that incorporates the tube, vehicle, propulsion system, suspension system, energy management, timing, and route. There is the possibility to build a passenger plus vehicle Hyperloop, but the main focus here will be on the passenger-only concept. The following is an overview of the Hyperloop components as defined by the alpha document. The alpha outline provided the basis for a top-down systems engineering analysis. Each subsystem was broken down into its fundamental parameters and governing physical principles. These were then analyzed to evaluate their effect on both the corresponding subsystem and the overall Hyperloop performance. Appendix A should be consulted for the important parameters of the Hyperloop system defined in the alpha document. These parameters were used to develop a detailed discussion of the Hyperloop in the following chapters.

2.1 Technical Components and Principles

2.1.1 Aerodynamic Drag

Tube Pressure

The Hyperloop capsule will be transported in a partially evacuated cylindrical tube supported by pillars in a closed system. For a capsule moving in a tube with air, the greatest power requirement is to overcome air resistance. Since aerodynamic drag increases with the square of the speed, the power requirement increases with the cube of the speed. To reduce the drag force and manage shock waves as the capsule approaches the speed of sound, the operating tube pressure is set to 100 Pa (1000

times less than sea level conditions). Further reducing the tube pressure would be offset by increased pumping complexity (see Chapter 7).

Tube and Capsule Geometry

The aerodynamics of the system require the capsule to tube area ratio (blockage ratio) to be as small as possible in order to best reduce the risk of choking the flow and to minimize the amount of power required to reach and maintain capsule speed. The capsule must displace its own volume of air as it moves through the tube and any flow that is not displaced may accelerate to supersonic velocities through the constricted gaps between the capsule and the tube, forming shock waves. Choking the flow and the formation of shock waves should be avoided as the required power will increase significantly to overcome the increased drag and additional mass of air in front of the vehicle. A compressor mounted on the capsule's leading face will ingest air that is not displaced, mitigating these adverse effects. In addition, the capsule's speed is limited to 760 mph in order to keep the flow subsonic for the given tube conditions.

The geometry of the capsule is streamlined to reduce drag (Figure 2.1). The frontal area is optimized to maximize speed and performance while maintaining passenger comfort. This corresponds to maximum width of 1.35 m and maximum height of 1.10 m. Not including any propulsion or suspension components this is equivalent to a frontal area of 1.40 m². The alpha document's optimized inner tube diameter is 2.23 m with a corresponding tube cross-sectional area of 3.91 m² and a blockage ratio of 36%.

2.1.2 Capsule Propulsion System

An advanced magnetic linear motor system will be developed to propel the vehicle to travel speeds. The system will be required to maintain passenger comfort while accelerating the capsule to 760 mph (339.75 m/s). To achieve this, the max acceleration is around 1g. For roughly 90% of the journey the capsule coasts and will not require propulsion. There will be several major propulsion stations along the journey to get the capsule up to speed as well as various reboost stations to maintain capsule speed. The tube will have a stationary element (stator) which powers the vehicle. The capsule will contain the moving rotor element (rotor). The rotors located on the capsule transfer momentum to the capsules via linear accelerators. The Hyperloop will be self-powering, using regenerative braking and solar power to reduce the energy requirements. A solar array will cover the entire tube with an expected energy

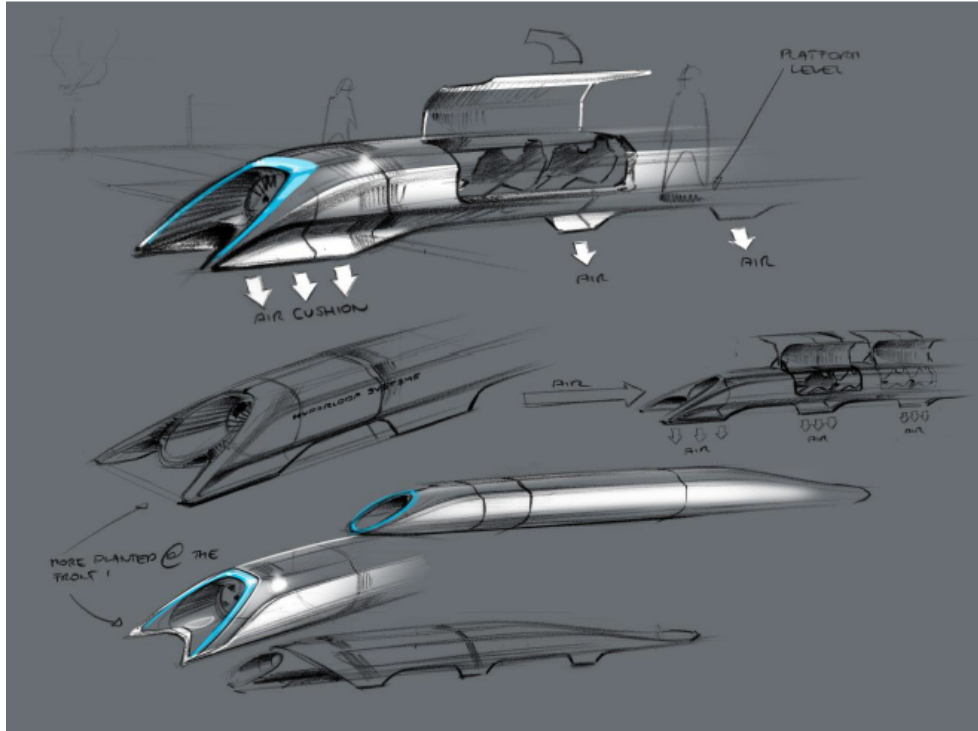


Figure 2.1: Concept sketch of Hyperloop capsule [34].

production of 120 W/m^2 . This will provide an annual average of 57 MW (76,000 hp), which is significantly more than the 21 MW (28,000 hp) the Hyperloop is described to require.

An emergency braking system will also be implemented. A possible aerodynamic way to stop involves isolating a section of the tube from the rest of the system and flooding it with air to quickly raise the pressure in this section. Other emergency braking methods will be pursued if faster braking is required.

2.1.3 Capsule Suspension System

The capsule suspension system is a major technical challenge of the Hyperloop. At the proposed high speeds a conventional wheel and axle system would be dynamically unstable and have huge frictional losses. Many other systems have proposed using magnetic levitation, but the material and construction costs are estimated to be too large. A feasible alternative is using an **air bearing suspension system**. **The capsule would sit on a cushion of air produced by pressurized air and aerodynamic lift.** By exploiting the ambient atmosphere in the tube, the cost is kept in check. This external pressure bearing offers stability (due to high stiffness) and extremely low drag. It is

also effective when stationary or moving at high speeds.

The design has air bearing skis floating on a pressurized cushion of air 0.50 mm to 1.30 mm off the tube's bottom surface. Using 28 of these suspension skis, only 9.4 kPa is needed to support the passenger capsule. The flow field in the gap will exhibit a highly non-linear reaction when the gap height between a ski and the tube is reduced. A large restoring pressure results, pushing the ski away from the wall and back to its nominal ride height. The skis will be constructed from iconel, a trusted alloy of SpaceX that is stiff and can withstand high pressure and heat. To eliminate any discomfort to passengers, each ski will be integrated into an independent mechanical suspension. The design also has the possibility of adding deployable wheels for speeds under 100 mph to ease movement and increase overall system safety.

A very sophisticated control system is needed for responding to the irregularities detected in the tube's surface as well as maintaining passenger comfort.

2.1.4 Vacuum Pumps

Vacuum pumps are necessary to first evacuate air from the Hyperloop tube before operation and to then maintain the desired pressure in the presence of any possible leaks throughout the tube. These pumps will run continuously along the length of the tube. Vacuum pumps will be selected based on pump-down time requirements. Any stations, emergency exits, or branches along the Hyperloop will be isolated from the main tube to minimize air leaks.

2.1.5 Compressor

A factor limiting the high speed movement of the Hyperloop capsule through a tube containing air is the Kantrowitz limit [61]. For a given tube to pod ratio there is a maximum speed that will choke the flow. If the capsule is too close to the tube's walls then the capsule will eventually be forced to push the entire column of air in the system. The Kantrowitz limit constrains the system to either go slowly or have a very large tube diameter, neither of which are ideal. The proposed solution is to mount an electric compressor fan on the nose of the pod that will actively transfer high pressure air from the front to the rear of the capsule. Throughout the journey the weight of the capsule will be supported by an air bearing system and this compressor will also serve to supply the necessary pressurized air.

2.1.6 Hyperloop Route

The proposed alpha route from Los Angeles to San Francisco will follow I-5 and I-580 for the majority of the 563 km journey. The minimum bend radius to maintain passenger comfort will dictate the speed of the capsule in each section of the route. The three cruising speeds of the capsule are 300 mph (134.11 m/s), 550 mph (248.11 m/s), and 760 mph (339.75 m/s). Propulsion stations are used to accelerate the capsule to each of these speeds and regenerative braking stations are then used to decelerate the vehicle. The journey will take 35 minutes one way. Capsules will be separated by 37 kilometers or depart roughly every 2 minutes. The passenger Hyperloop can carry up to 28 people and will transport 7.4 million people per year.

2.1.7 Infrastructure

Tube Construction

The inner diameter of the tube will be constructed from a uniform thickness steel tube reinforced with stringers. To provide sufficient strength for such load cases as pressure differential, bending and buckling between pillars, loading due to the capsule weight and acceleration, and seismic conditions the tube thickness should be between 20 mm and 23 mm. The inside of the tube will be finished to a smooth gliding surface using a specifically designed cleaning and boring machine.

Pylon Construction

The tube will be built on reinforced concrete pylons 6 m tall placed every 30 m to keep material cost and deflection to a minimum. They will not be rigidly fixed as there are two adjustable lateral (XY) dampers and one vertical (Z) damper. They are constructed to withstand earthquakes and have expansion joints. Slip joints at stations will be able to handle the tube length variance due to thermal expansion.

The tube is built above ground on pylons which allows prefabricated sections to be dropped in place. The tube can follow I-5 to avoid buying large amounts of land.

2.2 Total Cost Overview

2.2.1 Estimated Capsule Cost and Weight

The alpha document's estimations for an individual capsule's cost and mass can be found in Table 2.1.

Table 2.1: Estimated capsule cost and mass breakdown.

Vehicle Component	Cost (\$)	Mass (kg)
Capsule Structure & Doors	\$ 245,000	3100
Interior & Seats	\$ 255,000	2500
Propulsion System	\$ 75,000	700
Suspension & Air Bearings	\$ 200,000	1000
Batteries, Motor & Coolant	\$ 150,000	2500
Air Compressor	\$ 275,000	1800
Emergency Braking	\$ 50,000	600
General Assembly	\$ 100,000	N/A
Passengers & Luggage	N/A	2800
Total/Capsule	\$ 1,350,000	15000
Total for Hyperloop	\$ 54,000,000	

2.2.2 Total System Capital Costs

Two one-way tubes plus 40 capsules will cost \$6 billion incorporating a \$0.5 billion cost margin (Table 2.2). The capsules are only 1% of the total budget. The tubes represent 70% of the budget, or \$4.06 billion. The estimated total cost is only 9% of the California high speed rail. The service life will be 100 years.

A passenger plus transport version (Table 2.3) will only cost 25% more (still only 11% of the cost of the high speed rail).

Table 2.2: Estimated total cost of Hyperloop passenger transportation system.

Component	Cost (million USD)
Capsule	54 (40 capsules)
Structure & Doors	9.8
Interior & Seats	10.2
Compressor & Plumbing	11
Batteries & Electronics	6
Propulsion	5
Suspension & Air Bearings	8
Components Assembly	4
Tube	5,410
Tube Construction	650
Pylon Construction	2,550
Tunnel Construction	600
Propulsion	140
Solar Panels & Batteries	210
Station & Vacuum Pumps	260
Permits & Land	1,000
Cost Margin	536
Total	6,000

Table 2.3: Estimated total cost of Hyperloop passenger plus vehicle transportation system.

Component	Cost (million USD)
Cargo Capsule	30.5 (20 capsules)
Capsule Structure & Doors	5.5
Interior & Seats	3.7
Compressor & Plumbing	6.0
Batteries, Motor & Electronics	4.0
Propulsion	3.0
Suspension & Air Bearings	5.3
Components Assembly	3.0
Passenger Only Capsule	40.5 (30 capsules)
Capsule Structure & Doors	7.4
Interior & Seats	7.6
Compressor & Plumbing	8.2
Batteries, Motor & Electronics	4.5
Propulsion	3.8
Suspension & Air Bearings	6.0
Components Assembly	3.0
Tube	7,000
Tube Construction	1,200
Pylon Construction	3,150
Tunnel Construction	700
Propulsion	200
Solar Panels & Batteries	490
Station & Vacuum Pumps	260
Permits & Land	1,000
Cost Margin	429
Total	7,500

Chapter 3

Aerodynamic Analysis of the Hyperloop

3.1 Overview

The aerodynamic drag acting on the Hyperloop capsule as it travels through the tube depends on many factors. Numerical simulations using MATLAB¹ were used to investigate the effect of tube air pressure, capsule speed, capsule shape, and blockage ratio. Appendix A should be consulted for the important parameters of the Hyperloop system defined in the alpha document.

3.2 Introduction

Traditional trains are constrained to low speeds because a large percentage of the system energy is lost to the dynamic friction between the wheels of the train and the track rail. Maglev trains were introduced and designed to avoid this friction by floating above the track using magnetic levitation technology. Despite improvements, the velocity of the trains only achieved maximum commercial speeds of 400 - 500 km/hr. At these speeds aerodynamic drag is very high, about 80-90% of the total drag [29]. If drag could be reduced, then the speed of the vehicle could be increased. Evacuated tube transport (ETT) provides a solution to this problem by substantially reducing the pressure in the tube. In theory, an absolute vacuum would have zero

¹MATLAB was used for the analyses, results, and figures seen throughout all chapters

aerodynamic drag. While this is not feasible, low pressures 1000 times lower than atmospheric pressure can be achieved using current vacuum pump technology (see Chapter 7) and the shape of the vehicle can be further optimized to achieve very low drag forces. Simulations using the Navier-Stokes equation of compressible viscous flow and turbulence models such as k- ϵ can be implemented. To study the effect of aerodynamic drag in the evacuated tube of the Hyperloop, the basic mass conservation and momentum conservation equations were used to develop expressions for the total drag on the Hyperloop capsule as a function of desired parameters.

3.3 General Flow Analysis

The flow environment of the tube is very important and the following parameters can help evaluate the flow.

The speed of sound for a calorically perfect gas is given by ²

$$v_c = \sqrt{\gamma RT} \quad (3.3.1)$$

where γ is the ratio of specific heats, R is the specific gas constant, and T is the fluid temperature.

The Mach number helps to characterize the flow regime. For a fluid with velocity u_e , the Mach number is defined as

$$M = \frac{u_e}{v_c} \quad (3.3.2)$$

The Reynolds number is a measure of the ratio of inertia forces to viscous forces. This powerful non-dimensional parameter is helpful for predicting laminar or turbulent flow, and it is defined as

$$Re = \frac{\rho u_e h}{\mu} \quad (3.3.3)$$

where ρ is the fluid's density, μ is the fluid's dynamic viscosity, and h is the characteristic length.

For a fluid flow of $u_{e,max} = 339.75$ m/s and a tube temperature of $T_\infty = 293.15$ K, the speed of sound is $v_c = 343.20$ m/s and the Mach number is $M = 0.99$. Thus, at the alpha max speed the flow is just subsonic. Special attention needs to be paid to speed of sound locally, the effect of shock loss, and pressure recovery.

² v_c is used instead of the conventional symbol a to avoid confusion with other variables

3.4 Aerodynamic Drag Model

The geometries of the tube and capsule were simplified in order to observe overall trends of characteristic parameters. In Figure 3.1 the width and height of the tube are defined by a_0 , b_0 , respectively; the width, height, and length of the capsule are a , b , c , respectively.³ To make the model approximation consistent with the dimensions of the tube $a_0 = b_0 = 0.785 D_{tube}$ (this makes the cross sectional area of the square tube model equal to that of the circular pipe with diameter D_{tube}). The capsule is suspended above the bottom the tube by h (suspension gap height).

The blockage ratio, b_r , is defined by

$$\frac{ab}{a_0 b_0} = \frac{SA}{SA_0} \tag{3.4.1}$$

where SA and SA_0 are the frontal surface area of the capsule and the yz -cross sectional surface area of the tube, respectively.

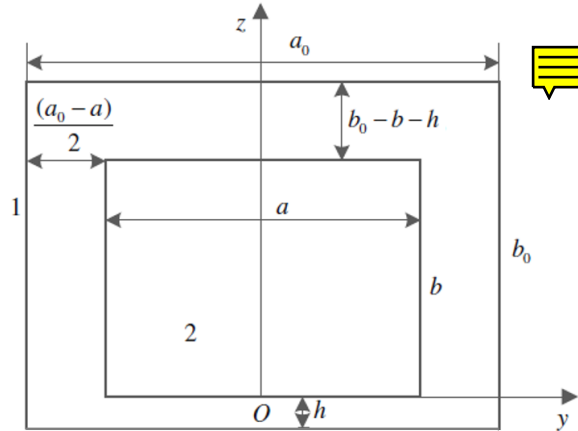


Figure 3.1: Aerodynamic model schematic of yz -cross section of Hyperloop capsule and tube.

The following assumption were made:

1. The capsule only moves in the x -direction.
2. The pressure is constant in the z -direction of the inner tube and the atmospheric molecular mass is neglected.
3. The capsule is in the center of the tube.

³ $a = W_{capsule}$, $b = H_{capsule}$, and $c = L_{capsule}$

Examining the mass and momentum conservation equations in the x-direction for an infinitesimal fluid element

$$\frac{\partial \rho(x, t)}{\partial t} + \nabla \cdot (\rho v_x) = 0 \quad (3.4.2)$$

$$\frac{\partial [\rho(x, t) v_x]}{\partial t} + \nabla \cdot [\rho(x, t) v_x^2] = \nabla \cdot (\mu \nabla v_x) - \frac{\partial p}{\partial t} + f_x \quad (3.4.3)$$

where ρ is the air's density in the tube, v_x is the capsule's velocity in the x-direction⁴, μ is the dynamic viscosity of the air in the tube, and f_x is the external force per unit volume acting on the fluid element in the x-direction. A streamlined nose of the capsule is not considered in this derivation in order to just highlight the effects of pressure in the tube, capsule speed, and blockage ratio.

There are three components of the capsule's drag that are considered.⁵

1. F_1 : The force on the front of the capsule due to the collision between air and the vehicle (only for velocities greater than the speed of sound)
2. F_2 : The air friction on the four faces of the capsule
3. F_3 : The force caused by the pressure differential between the front and rear of the capsule

3.4.1 F_1 Derivation

After air collides with the front of the capsule it will displace a small layer a short distance dx away in a small time dt . Thus, the velocity of this thin layer of air will change dt after the collision. The velocity of the infinitesimal air before the collision is equal to zero. Its velocity after the collision is equal to the capsule's. The kinetic energy of the air can be equated to the force differential times the distance traveled following the collision.

$$\frac{1}{2} \rho dx dy dz \cdot v_x^2 = dF_{1x} dx \quad (3.4.4)$$

Due to Brownian motion F_1 is equal to zero when the velocity of the capsule is less than the speed of sound (v_c). When the velocity is greater than v_c the air column with length $v_c \cdot dt$ is affected such that its velocity is approximately equal to the capsule's velocity. Combining these formulations with the momentum equation yields

⁴ v_x and u_e will be used interchangeably depending on the frame of reference

⁵Aerodynamic drag model was adapted from Ma et al. (2013)

$$F_1 = \begin{cases} 0 & v_x < v_c \\ -v_c \iint_{yz} \frac{p}{2p_0} \rho_0 v_x dydz & v_x \geq v_c \end{cases} = \begin{cases} 0 & v_x < v_c \\ -b_r SA_0 \frac{p}{2p_0} \rho_0 v_c v_x & v_x \geq v_c \end{cases} \quad (3.4.5)$$

where $p_0 = 101,325$ Pa, and $\rho_0 = 1.293$ kg/m³

3.4.2 F_2 Derivation

Friction force due to air is generated on the four faces of the capsule. The fluid flow between all four faces and the tube wall will be approximated as Couette flow. This flow is defined as laminar flow of a viscous fluid in the space between two parallel plates, one of which is moving relative to the other. The tube wall is treated as the fixed surface and the capsule's face can be represented by a moving plate at the freestream velocity, $u_e = v_x$. Due to the no-slip condition, there can be no relative motion between the plate and the fluid. The moving plate exerts a shear stress τ on the fluid causing the fluid to move. Couette flow is a constant pressure flow.

Considering an infinitesimal volume on the capsule's upper surface, the velocity profile is a function of z ($v'_x = f(z)$) and the area of contact is $ds = dx dy$. From the x-momentum equation

$$\frac{\partial}{\partial z} \left(\mu \frac{\partial v'_x}{\partial z} \right) = 0 \quad (3.4.6)$$

And for constant viscosity, μ ,

$$\frac{\partial^2 v'_x}{\partial^2 z} = 0 \quad (3.4.7)$$

which corresponds to a linear velocity profile. Applying the boundary conditions

$$v'_x(z) = v_x \frac{z}{b - b_0 - h} \quad (3.4.8)$$

The velocity gradient is then,

$$\frac{\partial v'_x}{\partial z} = \frac{v_x}{b - b_0 - h} \quad (3.4.9)$$

The shear stress acting between the capsule and the tube wall is given by the rela-

tionship of the internal friction and the velocity gradient,

$$\tau = \mu_{tube} \frac{\partial v'_x}{\partial z} \quad (3.4.10)$$

The shear force can then be integrated over the area of contact,

$$F_{2U} = -\mu_{tube} dx dy \quad (3.4.11)$$

The friction forces acting on the other three surfaces can be determined in a similar manner and thus,

$$F_2 = F_{2U} + F_{2B} + F_{2L} + F_{2R} \quad (3.4.12)$$

The bottom gap is very small and a temperature rise will be observed, resulting in a different viscosity (μ_{gap}) from the surrounding tube (μ_{tube}). Recognizing this viscosity difference and evaluating the integrals over the defined surface of each face results in

$$F_2 = -cv_x \left[\mu_{tube} \left(\frac{a}{b_0 - b - h} + \frac{2b}{\frac{1}{2}(a - a_0)} \right) + \mu_{gap} \frac{a}{h} \right] \quad (3.4.13)$$

3.4.3 F_3 Derivation

There will be a pressure differential between the front and rear of the Hyperloop capsule as it moves through the tube (Figure 3.2). The pressure inside the tube is p . Using the capsule as reference, the velocity of the infinitesimal fluid element is v_x . From Bernoulli's formula, the pressure at point A is defined as

$$p_{31} = p + \frac{1}{2} \rho v_x^2 \quad (3.4.14)$$

and the pressure at point B, neglecting any additional pressure due to the thrust gained from the exit of the onboard compressor, is

$$p_{32} = p \quad (3.4.15)$$

This pressure differential produces the force,

$$F_3 = - \iint_{yz} \frac{1}{2} \rho v_x^2 dy dz \quad (3.4.16)$$

Evaluating this integral yields,

$$F_3 = -b_r S A_0 \frac{\rho \rho_0}{2\rho_0} v_x^2 \quad (3.4.17)$$

The total drag force acting on the capsule in the x-direction is then

$$F_{drag,x} = F_1 + F_2 + F_3 \quad (3.4.18)$$

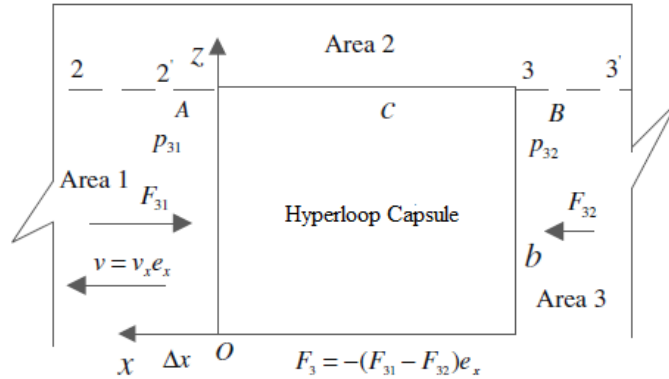


Figure 3.2: Schematic diagram for F_3 derivation

3.5 Numerical Analysis

Using MATLAB, plots were produced to demonstrate the effect of changing pressure, velocity, and blockage ratio on the total aerodynamic drag.

Figure 3.3 and 3.4 demonstrate the effect of increasing pressure and capsule velocity. In Figure 3.3, the velocity ranges from 0 to 400 m/s and the pressure ranges from 0 to 10,000 Pa. From the bottom leftmost plot it is evident that F_1 only has an effect once the capsule speed exceeds the speed of sound ($v_c = 343.2$ m/s). In addition, this force increases with both velocity and pressure. Despite not accurately modeling the impact of shocks once the capsule's travel becomes supersonic, the negative effects of reaching these speeds can still be observed in the large step increase in the total aerodynamic drag (top plot) due to F_1 . Only subsonic travel is considered for the Hyperloop and thus, F_1 will not be considered beyond this point. The plot of the air friction contribution to drag reveals a linear increase with the speed and no pressure dependence. Force due to the pressure differential is impacted more drastically by

the increase in pressure and speed. While the friction forces only reach levels of 10^2 Newtons, the pressure differential force rises to 10^5 Newtons. Clearly, to reduce drag the contribution due to pressure differential needs to be decreased by evacuating the tube to a low pressure.

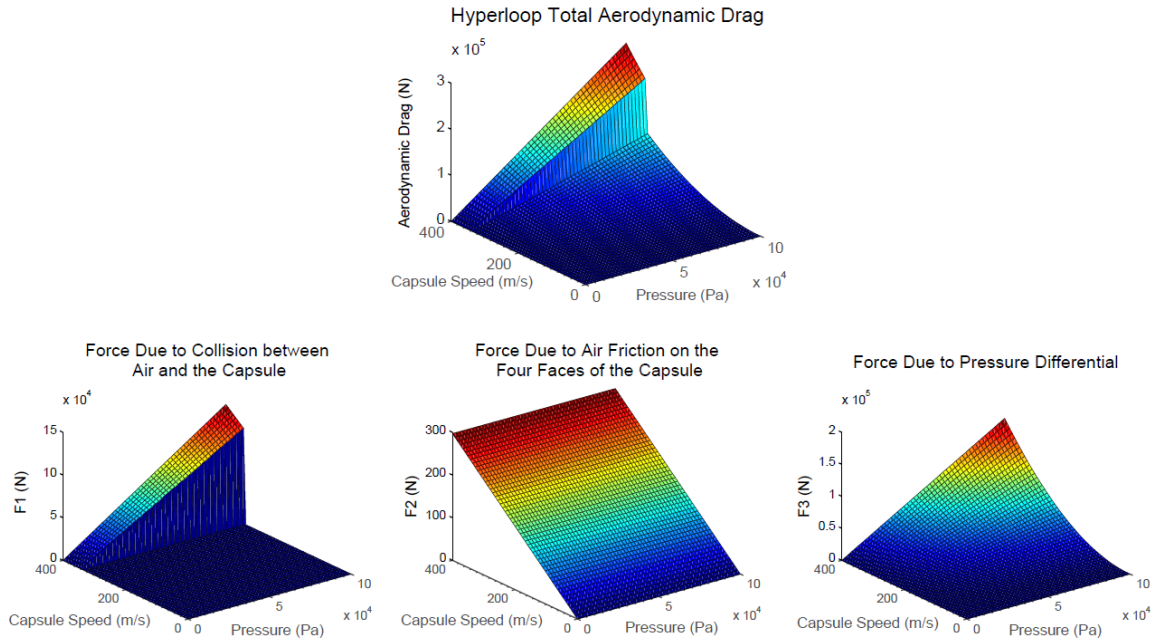


Figure 3.3: Aerodynamic Drag as Function of Tube Pressure and Capsule Velocity. The top plot is the total aerodynamic drag acting on the Hyperloop capsule. The three plots beneath show the contours for the three force components. The leftmost plot shows F_1 , the center plot shows F_2 , and the right plot shows F_3 .

Figure 3.4 examines the aerodynamic drag relationship with pressure and velocity only in pressure ranges that would be implemented in the Hyperloop. From the surface plot it is evident the drag force due to pressure is substantially less. It is only 800 N at maximum speed and 600 Pa (6 times the tube pressure proposed by the Hyperloop). The total drag force is substantially reduced. Figure 3.5 shows the aerodynamic drag as a function of pressure for the alpha document conditions. For the Hyperloop’s 100 Pa environment and at max velocity of 339.75 m/s, the total drag is only 362 N, which is at a magnitude that will allow the capsule to coast for most of its journey. The aerodynamic drag force’s effect on the capsule’s speed and position as a function of trip time can be examined in Chapter 9. Reducing the pressure to 0 Pa will give the lowest obtainable drag, but this is not feasible. For all three alpha speeds, further reducing the pressure below 40 Pa does not reduce drag by a substantial amount to warrant using more complex vacuum pump stations to achieve a lower pressure.

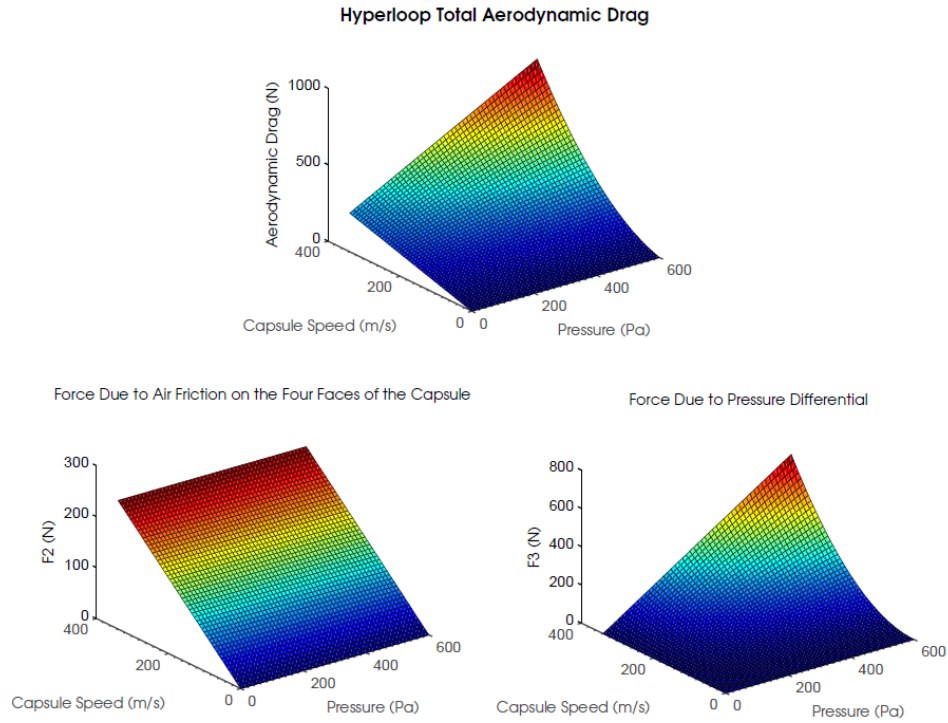


Figure 3.4: Aerodynamic Drag as a Function of Tube Pressure and Capsule Velocity. The drag is substantially lower when the pressure range is narrowed down to 0 to 600 Pa.

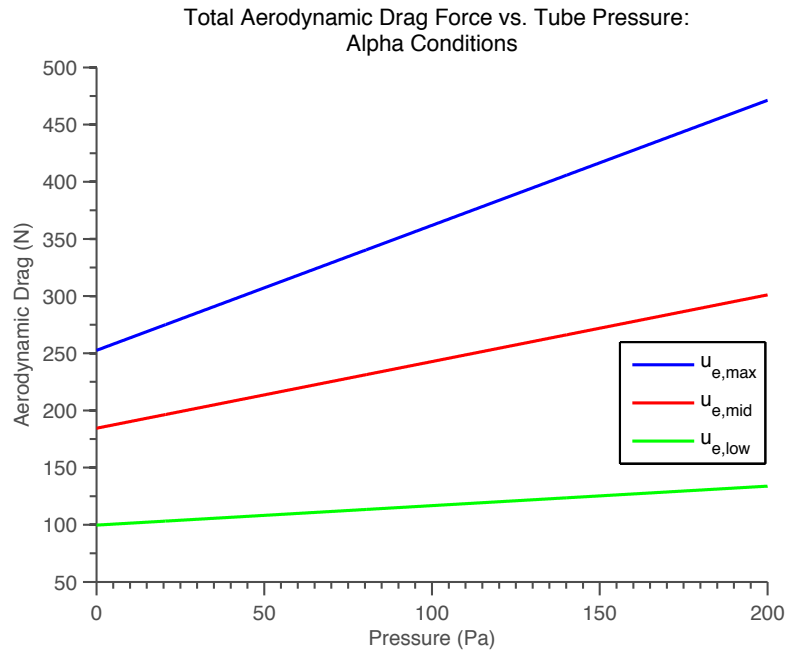


Figure 3.5: Aerodynamic drag as a function of tube pressure for alpha document conditions. Suspension gap = 1.3mm and $u_{e,max} = 339.75$ m/s, $u_{e,mid} = 248.11$ m/s, and $u_{e,low} = 134.11$ m/s

The effect of blockage ratio was then examined. The following were held constant and equal to alpha document specifications: all tube conditions, all bottom gap conditions (gap height = 1.3mm), the ratio of the capsule’s width to height, the capsule’s length, and the capsule’s velocity (taken to be $u_{e,max}$). Figure 3.6 demonstrates by increasing the blockage ratio the drag force increases. The drag force appears to start leveling off as b_r approaches 0.7. However, there is a point where the surface area of the capsule will be large enough to choke the flow at the Hyperloop’s high speeds. Once the flow has become choked, air will build up in front of the capsule and the aerodynamic drag will dramatically increase. This is not demonstrated as part of this particular analysis.

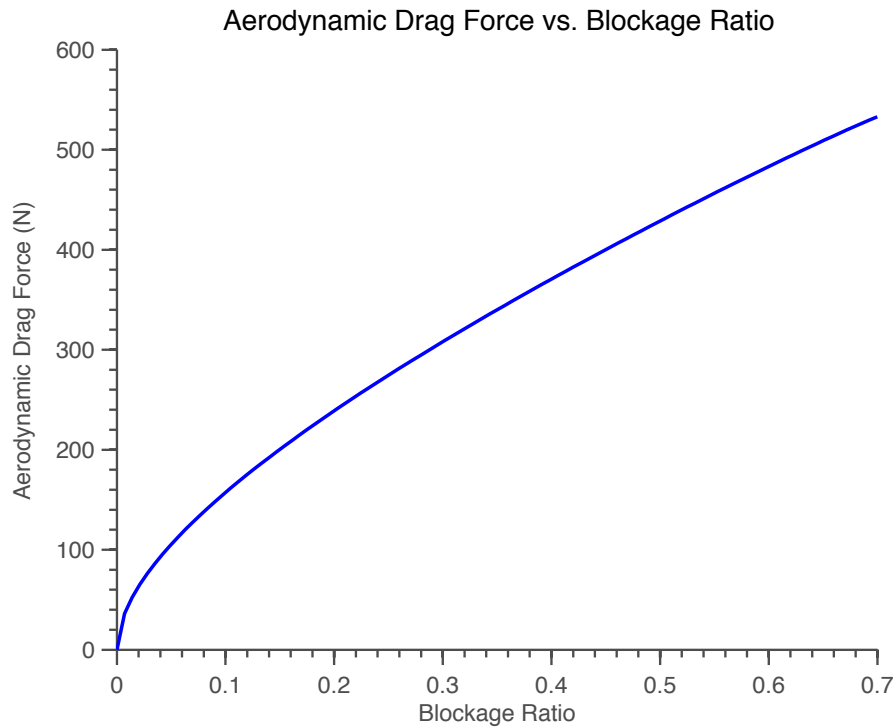


Figure 3.6: Aerodynamic Drag as Function of Blockage Ratio

3.6 External Studies

Several external studies have looked into the aerodynamic effects of a vehicle in an evacuated tube. Zhang (2011) considered a 40 meter subsonic Maglev train in an evacuated tube in feasible vacuum pressures of 1 to 1000 Pa. The research suggested the optimal blockage ratio for this form of ETT should be in the range of 0.25 to 0.70 and the tube diameter to be 2-4 meters [66].

Li et al. (2013) researched the thermal-pressure coupling effect on blockage ratio in the evacuated tube transportation system [28]. They developed thermal-pressure coupling equations based on the viscous Navier-Stokes equation and $k-\epsilon$ turbulence model for simulations. Although the study was for a tube pressure of 0.5 atm, the results should be similar at lower pressures. The results showed that when the speed of the vehicle and system pressure are held constant, the aerodynamic heating increases exponentially as the blockage ratio increases. Aerodynamic heating is caused by the vehicle friction with the surrounding medium at the high speeds. As the clearance between the capsule and the tube wall becomes smaller, more intense collisions and mixing of airflow occurs as well as more airflow viscous friction with the surface of the capsule, causing the temperature of the whole system to increase. A large amount of heat generation caused by the capsule can be harmful to the system's operation.

Zhang et al. (2012) considered the streamlined geometry of the ETT Maglev vehicle. They found the optimized taper length of the ETT train front/rear to be 1.5 – 2 times the train body section diameter [69]. Further increasing the taper only yields minimal decreases in aerodynamic drag. From their studies it was also apparent that tapering both the front and rear of the vehicle was more effective in reducing drag than just tapering the front (reduction by a factor of 2.3). The front/rear of normal high speed trains are designed to a ramp-up shape to reduce the lifting force acting on the train. In ETT, this effect is not desired, and instead a larger lifting force may be needed for which a vertical non-symmetrical front/rear with a more ramp-down shape may be designed.

The company Ansys used a high-end simulation software called Fluent to test out the Hyperloop's challenges with air flow, energy efficiency, and potential environmental damage with regard to the near-supersonic travel [54]. The shape of the capsule needs to be very carefully designed in order to operate the vehicle at subsonic speeds and keep the air flow from breaking the sound barrier. Figure 3.7 displays one of Ansys' initial rounds of computer simulations that showcases the air flow problems that may arise. The areas in red near the right side and back of the vehicle indicate high levels of shear stress, where the force pulling the vehicle backward would make the current designs energy inefficient. To minimize these red regions Ansys has suggested a more symmetric aerodynamic body. For example, the capsule should avoid tapering at the end. The projected velocity of the air flow around the Hyperloop in Figure 3.8 illustrates discrepancies in the proposed vehicle symmetry and the need for a more aerodynamic design. An improved design would allow for a more even pressure distribution across the outside of the vehicle and allow it to suck in more air.

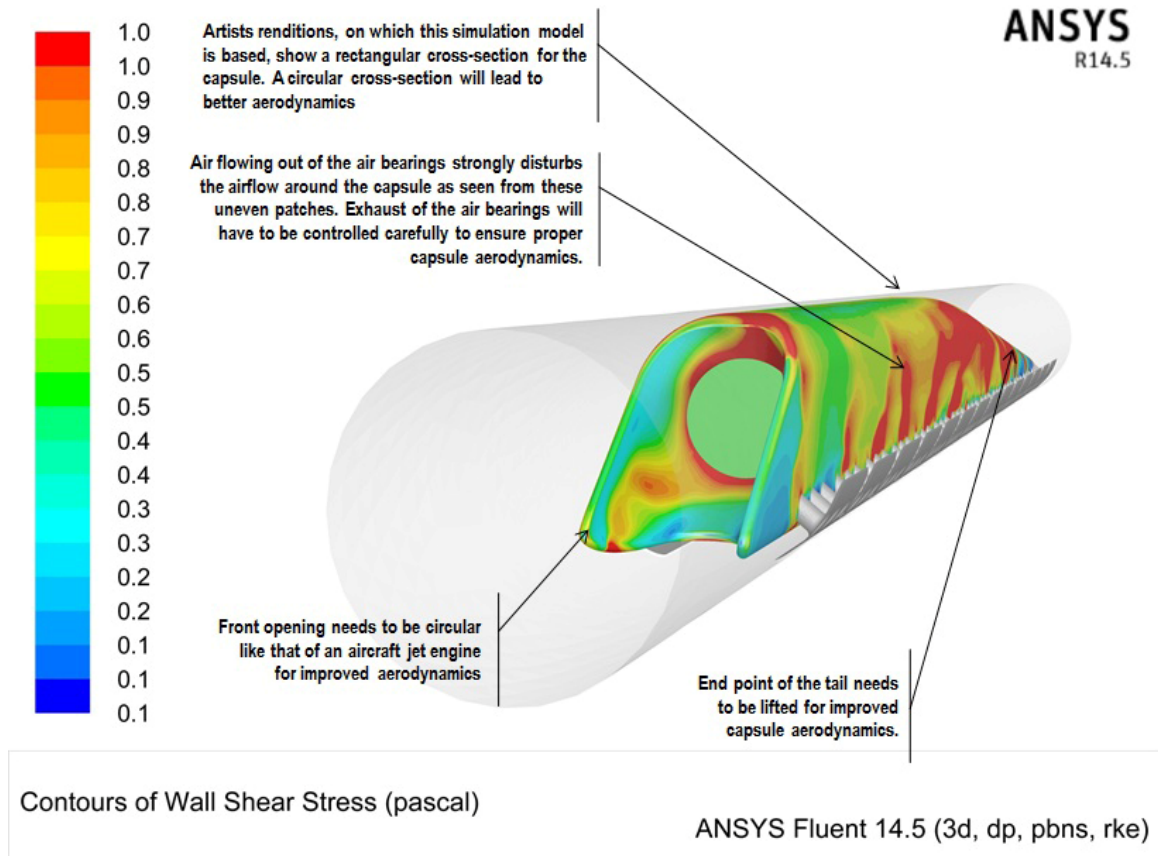


Figure 3.7: Ansys analysis of the Hyperloop: contours of wall shear stress (Pa).

Ansys has further suggested that adding air bearings to the top of the capsule would do a better job of spreading air across the body and help the vehicle stay balanced during slight changes in air pressure.

The simulation also revealed an issue with the amount of air sucked in by the front compressor and the release of that air. First, the converging nozzle at the front is causing some the flow to become supersonic. Adding a diffuser can slow the flow before it reaches the compressor. Second, to avoid flow becoming supersonic around the capsule and in the wake, more air needs to be sucked through the front fan. A significant amount of the air released will be directed to the air bearings to keep the capsule levitated. However, this potentially can disrupt the capsule's aerodynamics and lead to choked airflow. The placement of the air bearings and the amount of air flowing out will have to be carefully balanced.

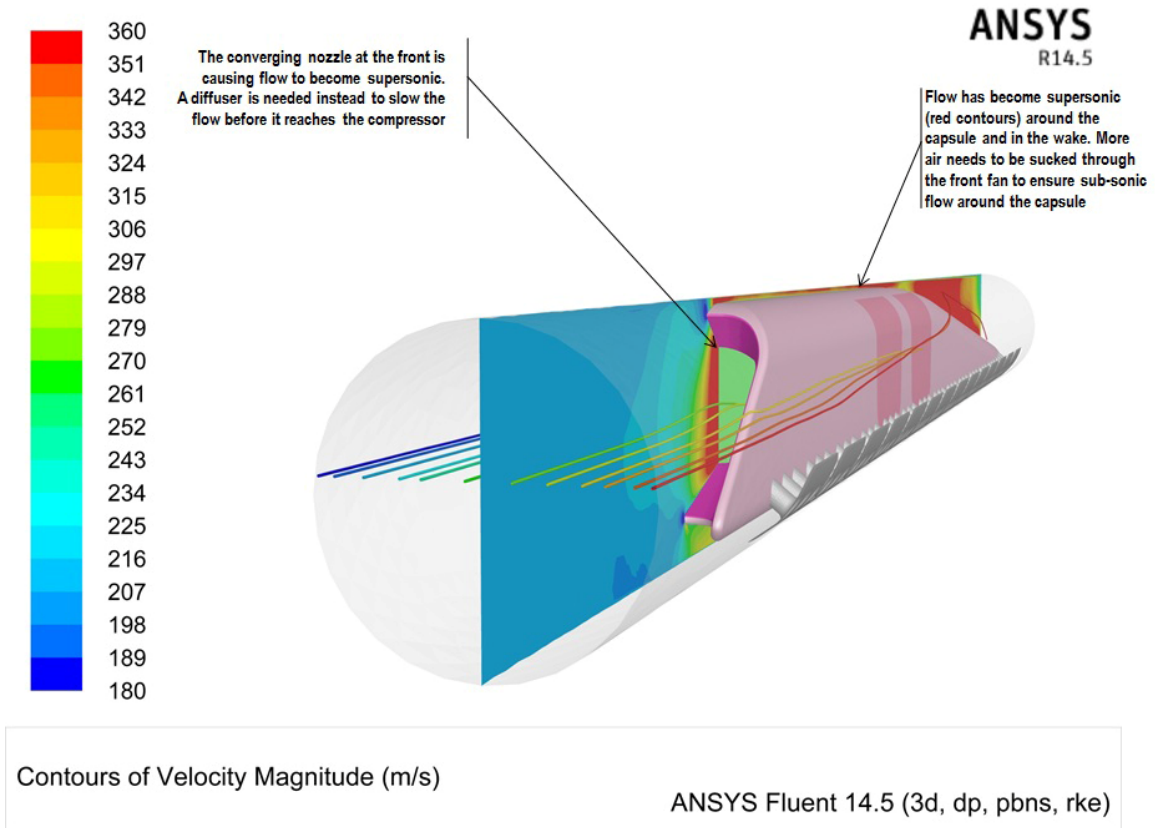


Figure 3.8: Ansys analysis of the Hyperloop: contours of velocity magnitude (m/s).

3.7 Summary

When the pressure and blockage ratio are held constant, the aerodynamic drag is a quadratic function of velocity. This becomes more complex when the speed of the capsule exceeds the speed of sound, and therefore, speeds will be limited to subsonic levels for the remainder of the thesis. At high tube pressures, the force due to the pressure differential dominates the total aerodynamic drag value. It is necessary to evacuate the tube to pressure levels around 100 Pa to reduce drag to a more manageable magnitude. This will allow the capsule to obtain higher speeds and longer coasting times. Chapter 11 will examine the effect of tube pressure on the overall Hyperloop trip time and more general conclusions will be drawn. In addition, for a fixed allowable drag, the lower the pressure the larger the allowable blockage ratio. Thus, for a given capsule size the tube can be smaller, reducing material costs. However, there is a trade-off between increasing vacuum costs and obtaining lower pressures (Chapter 7). For a given tube environment, the smaller the blockage ratio, the lower the drag. Again there will be a trade-off between decreasing blockage ratio

and the increasing costs of a larger tube diameter.

For a more in-depth study, Computational Fluid Dynamics needs to be used. Turbulence was ignored in the model discussed. The minimum Reynolds number ($Re = \frac{\rho u_e L}{\mu}$) for the alpha document tube conditions will be for the lowest speed ($u_{e,low}$), resulting in a value of 19,351. Because this is larger than 4,000, the flow is turbulent and turbulent models such as the k- ϵ should be used during CFD. In addition, the effects of the compressibility of air needs to be taken into account because the Mach number, M , is greater than 0.3.

Chapter 4

Propulsion Technology for the Hyperloop

4.1 Introduction

An advanced magnetic linear motor system will be developed to propel the Hyperloop vehicle to travel speeds. The system will be required to maintain passenger comfort while accelerating the capsule to 760 mph (339.75 m/s). To achieve this, the max acceleration will be limited to 1g for passenger comfort. For roughly 90% of the journey the capsule coasts and will not require propulsion. There will be several major propulsion stations along the journey to get the capsule up to speed as well as the potential to have various reboost stations every x-km to maintain capsule speed. The tube will have a stationary element (stator) which powers the vehicle. The capsule will contain the moving rotor element (rotor). The rotors located on the capsule transfer momentum to the capsule via linear accelerators.

4.2 The Linear Induction Motor (LIM)

4.2.1 Background

Linear motors are basically rotating motors that are cut and laid out flat. Instead of producing a torque, they generate a linear force along their length. Most commonly a linear motor operates as a Lorentz-type actuator [21]. Thus, the applied force is

linearly proportional to the magnetic field ($\mathbf{F} = I \mathbf{L} \times \mathbf{B}$). A linear induction motor is a type of AC asynchronous linear motor, typically with three-phase power supply to achieve balanced currents flowing in the stator windings. The stator (primary) is considered the field producing, non-moving portion of the motor, while the rotor (secondary) is moving element. When an external AC current is provided to the stator windings, an AC current is induced in the rotor in accordance to Faraday's law and a magnetomotive force (mmf) is generated in the rotor. Essentially, when the external magnetic field is moving faster than the superconducting rotor blade, it will pull the blade along and create the desired propulsion. The speed of the rotor is only limited by the frequency of the field, which can be very high, and by the air resistance. The limiting effects are minimal so very high speeds can be achieved. Advantages of induction motors include the ability to provide very high powers, the speed of the motor is nearly constant, low material costs (rotor can be simple aluminum shape), and easy maintenance (fewer moving parts)[15].

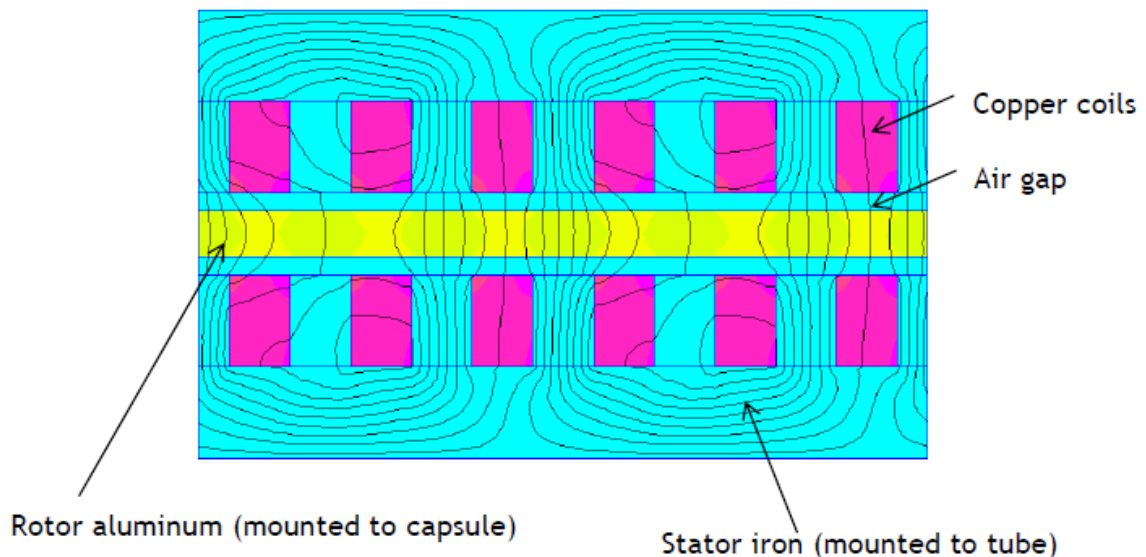


Figure 4.1: Double-Sided Linear Induction Motor (DSLIM) schematic with magnetic field strength inside the motor plotted [34].

The motor recommended for the Hyperloop is a Double-Sided Linear Induction Motor (DSLIM) (Figure 4.1). A DSLIM is a LIM with a primary on both sides of the secondary. The system benefits from having the field produced on both sides of the secondary and as a result there is a larger flux. In addition, double sides help balance the transverse forces acting on the rotor, keeping it aligned in the magnetic gap. These motors have been proposed as part of the Electromagnetic Aircraft Launch System

(EMALS) and will be implemented on aircraft carriers. A prototype of the EMALS was able to accelerate a 45,000 kg aircraft to 240 km/hr in only 91 m [25]. Substantial research is being directed into this technology as LIMs have historically had poor efficiencies. If the magnetic air gap can be reduced this will help improve efficiency. However, the high speed of motion between the **primary and secondary** prevents the air gap from being made too small in order to avoid contact. Flux leakage can also result when the air gap is large in comparison to pole pitch. A large amount of flux will bypass the secondary of the motor entirely and generate no useful power. The air gap also needs to be designed to account for thermal expansion and any torsion associated with operation or seismic activity. The following other problems limit LIM efficiency in comparison to conventional rotary motors: end effects due to the finite length of the rotor, transverse edge effects, spatial harmonics of the magnetic field, time harmonics of the supply current, and phase unbalances with the primary coils. Research has shown conventional rotary motors can have an efficiency around 90%, whereas linear motors are limited to an efficiency of 50% [26] [39]. **A MIT masters thesis written by Andrew P. Johnson (2005) established that Linear Induction Motors are capable of a maximum energy efficiency of 70% when operating at maximum effort [25].**

4.2.2 Hyperloop Alpha Propulsion Design

According to the Hyperloop alpha design conception, the rotor will be attached to the Hyperloop capsule (Figure 4.2). The alpha document listed the rotor being a 15 m long, 0.45 m tall, and 50 mm thick aluminum blade. The blade will be hollow to reduce weight and costs, allowing current to flow in the outer 10 mm of the blade. The distance between the rotor and stator (magnetic air gap) will be 20 mm on each side of the rotor. The alpha document recognized that a precise control system with electromagnetic centering would be needed to ensure the rotor safely enters, stays within, and exits the precise magnetic air gap. The projected weight was stated to be 1300 kg per capsule.

The stator will be mounted to the bottom of the tube. It will be 0.5 m wide, including the magnetic air gap, 10 cm tall, and weigh 800 kg/m. The length of the propulsion track runs 4 km. It will have a DSLIM configuration—stator is laid out symmetrically on each side of the rotor, its electrical configuration is a 3-phase, 1 slot per pole per phase, with a variable linear pitch (0.4 m max). The number of turns per slot also varies along the length of the stator, allowing the inverter to operate at

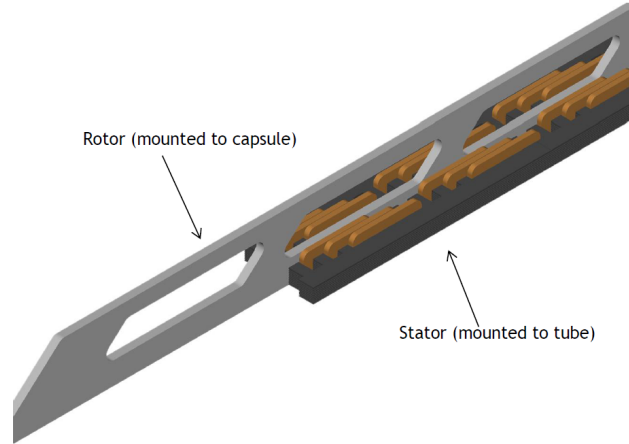


Figure 4.2: Hyperloop rotor and stator configuration [34].

nearly constant phase voltage, which simplifies the power electronics design. Because the two halves of the stator have an attractive magnetic force, braces will be required to keep them from coming together.

An energy conversion and storage system was also proposed by the alpha document. While the details will not be discussed, it is worth mentioning the alpha document expects the propulsion system to need an average power of 6 MW, which will be supplied by the solar arrays mounted to the tube's roof. An energy storage element capable of 38 MW-hr will be built out of the same lithium ion cells available in the Tesla Model S, allowing for the DSLIM to only draw average power from the solar array. Launching one capsule will only use 0.5% of the total energy in this unit.

4.3 Propulsion Analysis

At this stage in the Hyperloop system's analysis it is not necessary to include all the aspects of the Double-Sided Liner Induction Motor (DSLIM) in the propulsion models. Instead, it is more valuable to acknowledge this technology is a viable solution for propelling the Hyperloop capsule to speed and then focus on the general principles. This will allow for investigation into longitudinal g -forces on passengers, propulsion track length, propulsion times, propulsion energy, required peak power, regenerative braking, and general cost trends.

4.3.1 Propulsion Times and g -force Analysis

To ensure passenger comfort the maximum longitudinal acceleration during propulsion is limited to $1g$. The following analysis first uses the conditions stated in the alpha document to determine the amount of longitudinal g 's felt by riders. Then, the limiting conditions for an acceleration of exactly $1g$ are determined. Results are compiled in Table 4.1

In the alpha document the length of the propulsion track is stated to be 4 km for each major propulsion station. To find the g force under alpha document conditions the following relationship was developed from basic kinematic equations:

$$g_{force} = \frac{u_{e,2}^2 - u_{e,1}^2}{2d_{stator}}/a_{1g} \quad (4.3.1)$$

where $u_{e,2}$ and $u_{e,1}$ are the capsule's speed at the end of propulsion and at the start of propulsion, respectively; d_{stator} is the length of the propulsion track; and $a_{1g} = 1g = 9.81 \text{ m/s}^2$.

The time to to accelerate under alpha document conditions was again derived from kinematic relationships and is given below:

$$t_{\alpha} = \frac{2d_{stator}}{u_{e,2} + u_{e,1}} \quad (4.3.2)$$

Next, the limiting conditions for $1g$ acceleration were explored. Equation 4.3.3 calculates the minimum length of propulsion track needed to accelerate the capsule under constant $1g$ acceleration conditions.

$$d_{min} = \frac{u_{e,2}^2 - u_{e,1}^2}{2a_{1g}} \quad (4.3.3)$$

The minimum time to accelerate under $1g$ conditions is given by:

$$t_{min} = \frac{u_{e,2} - u_{e,1}}{a_{1g}} \quad (4.3.4)$$

Table 4.1: Hyperloop propulsion: g -force, minimum track length, alpha times, and minimum times.

Propulsion Segment	g force α	d_{min} (km)	t_α (s)	t_{min} (s)
0 mph to 300 mph	.2292 g	.9167	59.65	13.67
300 mph to 550 mph	.5552 g	2.22	20.93	11.62
550 mph to 760 mph	.6864 g	2.75	13.61	9.34
300 mph to 760 mph	1.24 g	4.97	16.88	20.96

4.3.2 Propulsion Work and Power

The work and power for propulsion are important. It is assumed that the propulsion can take place at constant acceleration, with $a = 1g$. The force the DSLIM needs to supply to the vehicle is found from Newton's second law and given below:

$$F_{prop}(t) = m_c g - F_{drag}[u_e(t)] \quad (4.3.5)$$

where m_c is the mass of the Hyperloop capsule and $F_{drag}[u_e(t)]$ is the aerodynamic drag (negative value) from Chapter 3 and is a function of capsule speed, $u_e(t)$.

The total work throughout the entire propulsion section is

$$\begin{aligned} W_{prop} &= \int_{t_i}^{t_f} F_{prop} \cdot u_e dt \\ &= \int_{t_i}^{t_f} (m_c g - F_{drag}[u_e(t)]) dt \end{aligned} \quad (4.3.6)$$

where t_i and t_f are the times at the start and end of propulsion, respectively. The total amount of work during propulsion will reveal the amount of energy required for each propulsion section.

From elementary physics, power is defined as $P = \frac{dW}{dt} = \mathbf{F} \cdot \mathbf{v}$. The average power for propulsion will indicate the operational costs, while the peak power is a constraint the system must be able to handle. The average power is defined by

$$P_{avg} = \frac{W_{prop}}{t_{prop}} \quad (4.3.7)$$

and the peak power required for propulsion is

$$\begin{aligned} P_{peak} &= F_{prop} \cdot u_{e,2} \\ &= (m_c g - F_{drag}[u_{e,2}]) \cdot u_{e,2} \end{aligned} \quad (4.3.8)$$

where $u_{e,2}$ is the final speed of the Hyperloop capsule at the end of propulsion.

In terms of electrical properties, the power supplied by the DSLIM is

$$P_{in,motor} = VI \quad (4.3.9)$$

where V is the electrical voltage (potential) supplied and I is the electrical current. The power required will dictate the electrical components used. High powers will require heavy duty conductors and have a larger amount of heat dissipation associated with them.

The efficiency of the DSLIM, η_{motor} , and the contributing sources of loss, especially magnetic gap size, was discussed previously. The maximum theoretical efficiency was found to be 0.7, but for this analysis η_{motor} is assumed to be 0.6. The degree of efficiency demanded will directly affect the magnetic gap designed which will impact tolerances and manufacturing costs. To propel the Hyperloop to the desired speed the power supplied must be,

$$P_{in,motor} = \frac{P_{avg}}{\eta_{motor}} \quad (4.3.10)$$

In addition, there will be an associated efficiency with the energy storage supply transmission, η_{trans} , which will be around 0.95 in the worst case. Thus, the total power supplied will need to be,

$$\begin{aligned} P_{in} &= \frac{P_{in,motor}}{\eta_{trans}} \\ &= \frac{(m_c g - F_{drag}[u_{e,2}]) \cdot u_{e,2}}{\eta_{motor} \cdot \eta_{trans}} \end{aligned} \quad (4.3.11)$$

Table 4.2 compiles the work and power requirements for 1g propulsion under alpha conditions with a suspension air gap of $h_{gap} = 1.3$ mm. The peak powers the system needs to be able to handle are shown in parenthesis next to the average powers. The results reveal peak powers on the same level as the alpha document (56 MW). However, the average powers computed are much higher than the alpha documents referenced 6 MW. The computed power becomes even higher when considering the

inefficiencies of the linear motor and the power transmission. It is possible the alpha document considers propulsion of each section at an acceleration less than $1g$ and therefore, the total time of propulsion is longer and the average power will be lower. The alpha document also stated that solar array covering the Hyperloop is large enough to provide an annual average of 57 MW with solar system having a 285 MW peak power total. The energy storage of the alpha system only plans to supply the average power (6 MW) to the propulsion, while including battery arrays at each accelerator to deal with the peak powers. MATLAB simulations also revealed that neither suspension gap height nor capsule frontal surface area have a large effect on average power and total work.

Table 4.2: Hyperloop propulsion work and power requirements for $1g$ acceleration.

Propulsion Segment	W_{prop} (MJ)	P_{avg} (MW)	P_{motor} (MW)	P_{trans} (MW)
0 mph to 300 mph	134.97	9.87 (19.75)	16.46	17.32
300 mph to 550 mph	327.24	28.16 (36.57)	46.93	49.40
550 mph to 760 mph	404.91	43.35 (50.12)	72.24	76.04
300 mph to 760 mph	732.15	34.93 (50.12)	58.21	61.28

4.3.3 Regenerative Braking

There is the potential to recover some energy using regenerative braking. A regenerative braking system uses a back-to-back converter, which allows bidirectional power flow. The electricity generated by the deceleration of the linear motor can be returned to the grid for later use or used by auxiliary systems. Thus, some of the power required to power a capsule through the Hyperloop can be drawn from the power saved from the braking of the previous capsule. If excess power from regenerative braking and solar panels exceeds the input needs, there is the potential for the power to be sold.

During regenerative braking, the load torque reverses its direction, but the operation direction remains the same. The kinetic energy from braking drives a motor and when synchronous speed is exceeded, mechanical power is converted into electrical. The power produced from regenerative braking from capsule speed $u_{e,1}$ to $u_{e,2}$ is given by

$$P_{regen} = \eta_{regen} \cdot \frac{m_c (u_{e,2}^2 - u_{e,1}^2)}{2\Delta t} \quad (4.3.12)$$

where the regenerative efficiency, $\eta_{regen} = \frac{W_{regen}}{W_{brake}}$, with W_{regen} being the amount of

brake energy converted into useful energy and W_{brake} the amount of pure brake energy. Typical efficiencies range between 0.6 and 0.7, and can even reach 0.85 [56].

The power and energy regenerated from braking from $u_{e,1}$ to a complete stop is examined. The regenerative power expression becomes:

$$P_{regen} = \eta_{regen} \cdot (m_c a_{brake} u_{e,1}) \quad (4.3.13)$$

The power supplied to an energy converter is equal to the power generated by regeneration ($P_{in,conv} = P_{regen}$). The energy converter will have a transmission efficiency, η_{trans} . The energy regained is thus,

$$E_{out} = \frac{\eta_{trans} \cdot \eta_{regen} \cdot m_c u_{e,1}^2}{2} \quad (4.3.14)$$

The power regeneration and energy recovered are plotted as functions of initial capsule speed, $u_{e,1}$ in Figure 4.3 and 4.4. It is assumed $\eta_{regen} = 0.6$ and $\eta_{conv} = 0.95$.

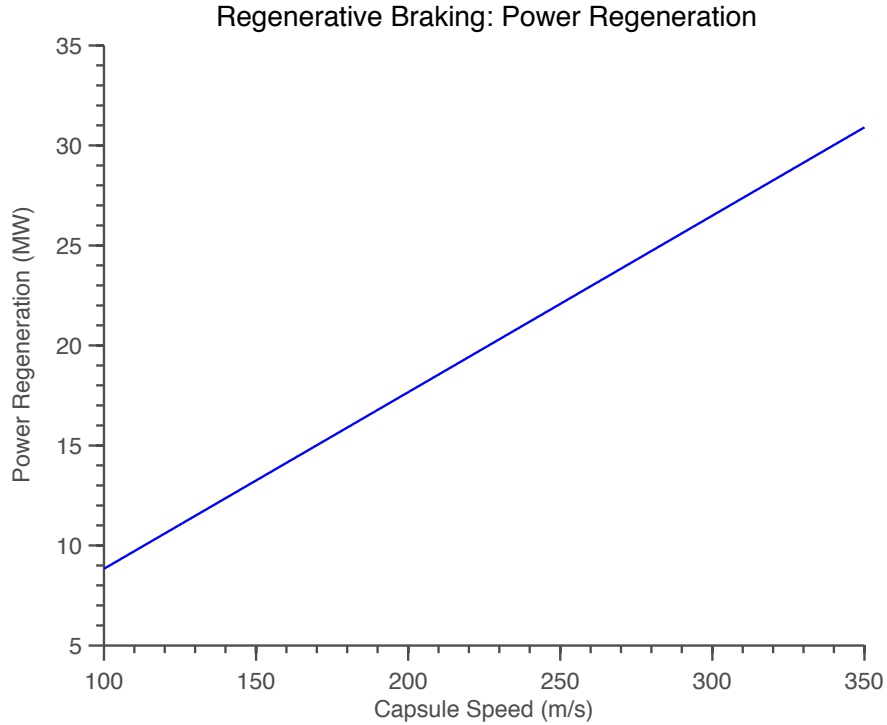


Figure 4.3: Regenerative braking: power as a function of initial capsule speed $u_{e,1}$.

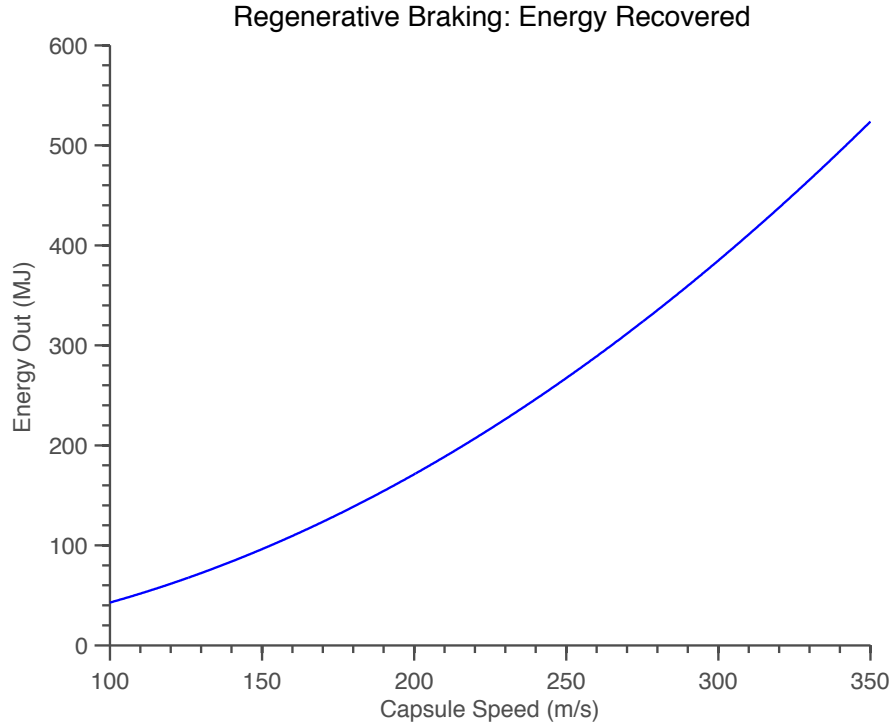


Figure 4.4: Regenerative braking: energy recovered as a function of initial capsule speed $u_{e,1}$.

For each of the four propulsion segments considered, assume as soon as the capsule reached desired speed regenerative braking was applied at $1g$ deceleration to the speed at the start of the propulsion segment. The percentage of input energy to propel the vehicle ($E_{prop,in}$) regained by the regenerative braking system (E_{regen}) is displayed in Table 4.3. About half the input energy can be recovered.

Table 4.3: Hyperloop regenerative braking energy recovery vs. propulsion energy.

Propulsion Segment	$E_{prop,in}$ (MJ)	E_{regen} (MJ)	Percent Recovered
0 mph to 300 mph	134.97	68.79	50.97%
300 mph to 550 mph	327.24	206.06	62.97%
550 mph to 760 mph	404.91	166.67	41.16%
300 mph to 760 mph	732.15	372.73	50.91%

4.3.4 Propulsion Costs

The alpha document breaks down the propulsion costs for the tube side in the following way:

- Stator and structure materials = 54%
- Power electronics (traction inverters, grid tie inverters) = 33%
- Energy Storage = 13 %

For a total of \$140 million USD.

On the capsule side, propulsion unit cost is estimated to be \$150,000 per capsule (\$6 million for a system with 40 capsules).

These numbers were used as a starting point to estimate the costs of the propulsion system. It is expected that the fewer propulsion stations, the lower the overall cost. The minimum number of stations is 6 per direction (3 for acceleration and 3 for deceleration) to ensure capsule is traveling at appropriate speed for the minimum track bend radius in that region of the track. The segments are 0 – 300mph, 300 – 550mph, and 550 – 760mph. The difference between the cost of a propulsion acceleration station versus a propulsion regenerative braking station was not discussed so it will be assumed they are the same. A revised breakdown of propulsion costs can be established by using the alpha costs as a baseline in combination with the computed average powers, track distances, and energy requirements for each propulsion segment under 1g conditions (this is carried out under the assumption the minimum number of stations was used in the alpha document’s assessment of propulsion capital costs). Stator and structure material costs depend on propulsion track length. The cost of power electronics is proportional to the average power requirements and the cost of the energy storage scales with the energy requirement. The results in Table 4.4 show the cost of each propulsion category per station.

Table 4.4: Hyperloop Propulsion Components Capital Costs Per Station - Tube Side.

Propulsion Segment	Stator and Structure (million USD)	Power Electronics (million USD)	Energy Storage (million USD)
0 mph to 300 mph	\$2.89	\$3.60	\$1.42
300 mph to 550 mph	\$6.99	\$8.72	\$3.44
550 mph to 760 mph	\$8.66	\$10.78	\$4.25

These numbers can be used to develop a capital cost for the minimum propulsion station case. In addition, the effect of adding more propulsion stations can be evaluated using these numbers. The estimated capital cost of tube side propulsion components is suggested to be \$101.5 million for the minimum propulsion segment case. It is interesting to note that the power electronics and energy storage compo-

nents are larger percentages of the overall propulsion costs than the alpha document while the stator and structure are a smaller percentage. This is because the power and energy requirements for the $1g$ case are very similar to the alpha case, whereas the the propulsion track is much shorter for the $1g$ case than the alpha case. In addition, not only does $1g$ reduce propulsion times from the alpha suggestions, the propulsion total capital costs for $1g$ are less than the proposed alpha costs. This suggests adding various small boost stations throughout the route can be achieved for a small increase in cost. If the track path can be altered such that the track bend radii are large, the 300 – 550mph and 550 – 760mph segments could be combined to a single 300 – 760mph section. This would save propulsion costs, yet it likely the amount of capital required to alter the track path so this is possible is extraordinary larger than the benefits of having less propulsion stations.

To evaluate operating costs, the average cost of electricity in the Los Angeles Area for 2013 was found to be \$0.214 per kW-hr (Bureau of Labor Statistics, 2014 [6]). Assuming the Hyperloop is operational for 12 hours a day, year-round with an average capsule departure of 2 minutes, then annual cost of operating the minimum 6 propulsion stations is \$6.77 million USD without regenerative braking and \$3.32 million USD with regenerative braking. These operational costs can be reduced by using a solar array. Assuming the solar array spans the length of the tube and generates an average of 57 MW annually, there is more than enough energy for propulsion. This additional energy could be sold for approximately \$100.08 – 103.53 million USD per year. A little over two years of operation could pay for the capital costs of the solar array and battery infrastructure (\$260 million USD). Because more than propulsion will need energy input (vacuum pumps for example) this number will be much lower, but still significant enough to sell and ultimately keep ticket prices low.

Chapter 5

Air Bearing Suspension System

5.1 Introduction

The capsule suspension system is a major technical challenge of the Hyperloop. At the targeted high speeds a conventional wheel and axle system would be dynamically unstable and have huge frictional losses. Most evacuated tube transport systems such as ET3 have proposed using magnetic levitation. While the literature is inconsistent reporting maglev component capital costs, they suggest the costs of the material and construction are large. If lower expenditures are desired, a feasible alternative is to use an air bearing suspension system. In this design the capsule would sit on a cushion of air produced by pressurized air and aerodynamic lift. By exploiting the ambient atmosphere in the tube, the cost is kept in check. This external pressure bearing offers stability (due to high stiffness) and extremely low drag. The air suspension is most effective when moving at high speeds as more lift is generated, while lower speeds require substantially more compressed air input from the air bearing ski to maintain levitation. Chapter 6 will then explore an in-depth analysis of the suspension system using a quarter car suspension system model with H_∞ control synthesis.

5.2 Alpha Design

The alpha design parameters will direct the analysis of the flow behavior in the suspension gap as well as the air bearing suspension system's feasibility and control.

The alpha document design has air bearing suspension skis floating on a pressurized cushion of air 0.50 mm to 1.30 mm off the tube's bottom (Figure 5.1). This

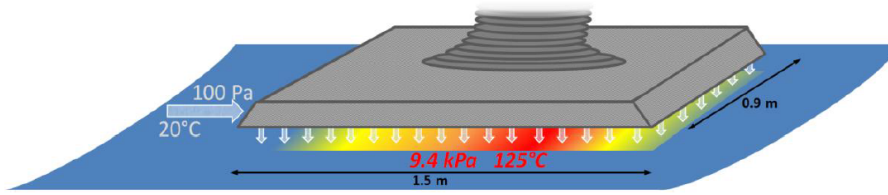


Figure 5.1: Alpha design schematic of air bearing skis that support the capsule [34].

distance is defined as the suspension gap height (h_{gap}). Due to the compression of air in the small gap and heat transfer, the temperature will increase ($T_{gap} = 398.15$ K) and effect the flow. The alpha team concluded only 9.4 kPa is needed to support the passenger capsule. The flow field in the gap will exhibit a highly non-linear reaction when the gap height between a ski and the tube is reduced. A large restoring pressure results, pushing the ski away from the wall and back to its nominal ride height. The skis will be constructed from iconel, a trusted alloy of SpaceX that is stiff and can withstand high pressure and heat. To eradicate any discomfort to passengers, each ski will be integrated into an independent mechanical suspension. The design also has the possibility of adding deployable wheels for speeds under 100 mph to ease movement and increase overall system safety.

The suspension parameters used during numerical analysis can be found in Table 5.1.

Alpha Suspension Parameter	Value
$h_{gap, min}$ (mm)	0.5
$h_{gap, max}$ (mm)	1.3
W_{ski} (m)	0.9
L_{ski} (m)	1.5
N_{ski}	28
α (deg)	0.5
p_{gap} (kPa)	9.3
T_{gap} (K)	398.15
μ_{gap} (N-s/m ²)	2.3185E-05

Table 5.1: Air suspension system parameters

5.3 Suspension Gap Flow Characteristics

5.3.1 Gap Temperature

The average gap temperature can be estimated from an adiabatic temperature loss computation,

$$T_2 = T_1 \left(\frac{V_1}{V_2} \right)^{\gamma-1} \quad (5.3.1)$$

$$= T_1 \left(\frac{h_1}{h_2} \right)^{\gamma-1} \quad (5.3.2)$$

where h_1 is the distance the front of the air bearing ski is off the bottom of the tube,

$$h_1 = h_{gap} + L_{ski} \sin(\alpha)$$

where α is the ski's angle of attack. h_2 is the distance the back of the air bearing ski is off the bottom of the tube,

$$h_2 = h_{gap}$$

T_1 is the temperature at the ski front ($T_1 = T_{tube}$) and T_2 is the temperature at the ski rear. The average temperature in the gap is thus,

$$T_{gap, avg} = \frac{1}{2} T_{tube} \left(\frac{h_{gap} + L_{ski} \sin(\alpha)}{h_{gap}} \right)^{\gamma-1} \quad (5.3.3)$$

Using $T_{tube} = 293.15$ K and the maximum gap, $h_{gap, max}$, the adiabatic temperature in the gap would be $T_{gap, avg} = 383.45$ K.

In reality, there will be heat transfers due to friction so the adiabatic conditions will not hold and the average calculation will not be appropriate. Correct analysis of the temperature will consider the viscous dissipation which depends on the velocity gradient in the gap. This will yield a value closer to what the alpha document presented. Thus, it is assumed $T_{gap} = 398.15$ K.

5.3.2 Knudsen Number and Flow Characterization

Due to the small gap size between the tube wall and the suspension ski, the value of the Knudsen number needs to be computed in order to determine whether the

continuum mechanics formulation of fluid dynamics or statistical mechanics should be used. The Knudsen number is defined as the mean free path between the freestream air molecules (λ) divided by the characteristic length through which the gas flows [22]. The number is used to signal the onset of the different regimes of free molecular flow. When the Knudsen number reaches about 0.03 the flow is characterized by velocity slip (the fluid velocity is no longer zero at the wall) and temperature slip (the gas temperature at the wall is no longer the surface temperature). At Knudsen numbers greater than 0.3 the continuum Navier-Stokes equations no longer apply. For the suspension gap flow, the characteristic length is taken to be h_{gap} and thus,

$$\begin{aligned} Kn &= \frac{\lambda}{h_{gap}} \\ &= \frac{k_B T_{gap}}{\sqrt{2} \pi \sigma^2 p_{gap} h_{gap}} \end{aligned} \quad (5.3.4)$$

where k_B is the Boltzmann constant and σ is the particle hard shell mean diameter ($\approx 3.7 \cdot 10^{-10}$ m for air). For the minimum gap height, the largest Knudsen value observed would be 0.002. Therefore, it is a valid assumption to use continuum fluid mechanics.

5.3.3 Couette Flow

Chapter 3 identified one of the contributing factors to the aerodynamic drag was air friction. Couette flow was used to describe the flow between the tube wall and the capsule. The tube wall is treated as the fixed surface and the capsule's suspension bearing ski can be represented by a moving plate at velocity u_e . Due to the no-slip condition, there can be no relative motion between the plate and the fluid. The upper plate exerts a shear stress τ on the fluid causing the fluid to move. For, incompressible flow the velocity profile was found to be,

$$u = u_e \frac{y}{h_{gap}} \quad (5.3.5)$$

The fluid flow profiles of the three main Hyperloop speeds are plotted for the minimum suspension gap height (0.5mm) in Figure 5.2 and for the maximum suspension gap height (1.3mm) in Figure 5.3. These figures reveal that Couette flow exhibits a linear profile.

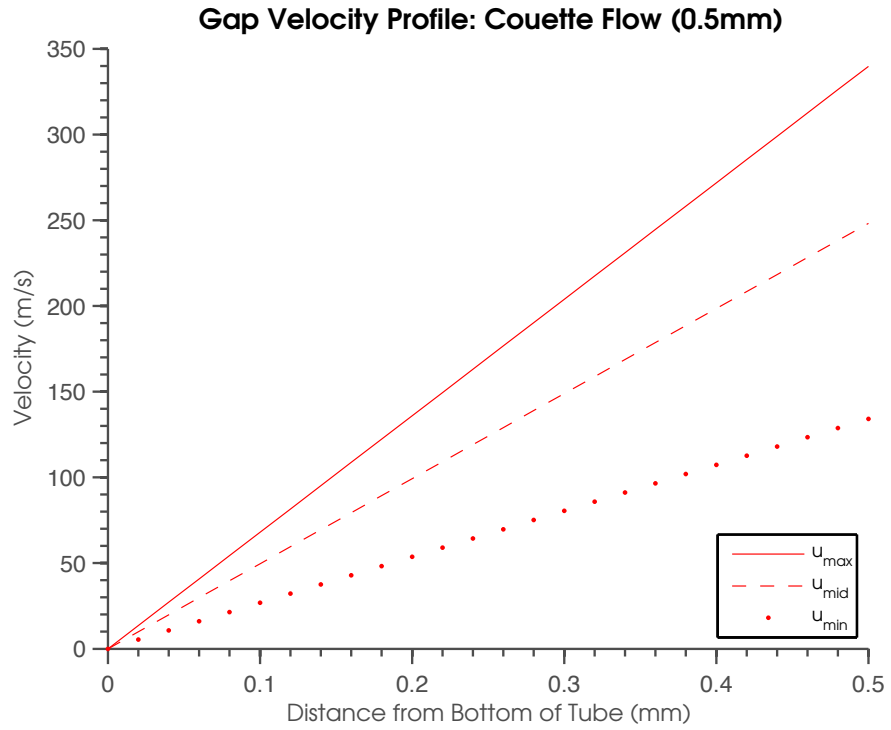


Figure 5.2: Couette flow analysis for gap = 0.5 mm and $u_{e,max} = 339.75$ m/s, $u_{e,mid} = 248.11$ m/s, and $u_{e,low} = 134.11$ m/s.

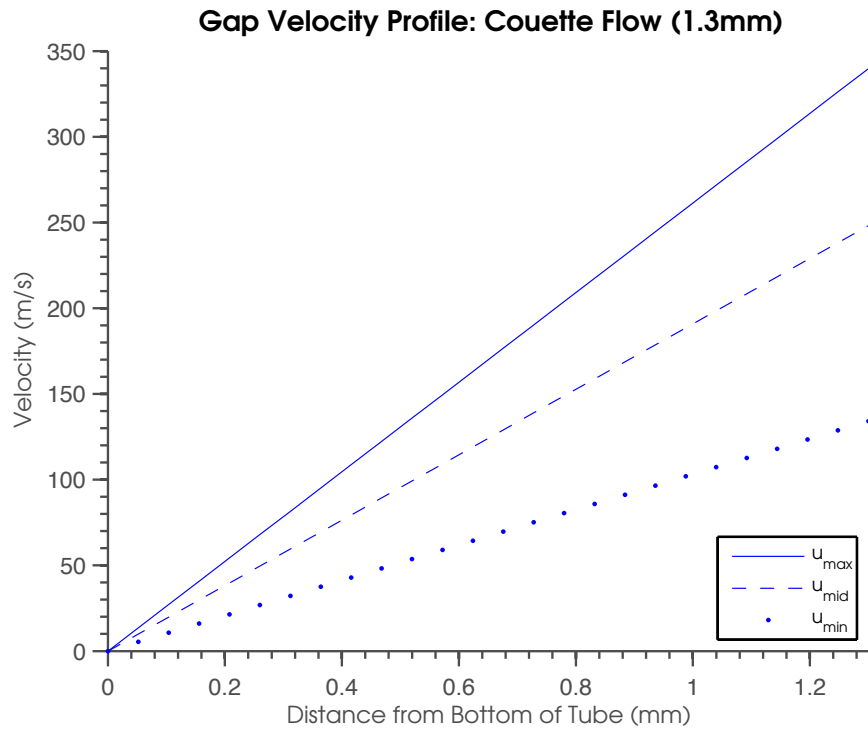


Figure 5.3: Couette flow analysis for gap = 1.3 mm and $u_{e,max} = 339.75$ m/s, $u_{e,mid} = 248.11$ m/s, and $u_{e,low} = 134.11$ m/s.

Newton’s viscous effect states that the shear stress in the fluid is proportional to the rate of change of velocity with respect to y . Thus, the shear stress is given by

$$\tau = \mu \frac{\partial u}{\partial y} \tag{5.3.6}$$

where μ is the dynamic viscosity, which is a measure of internal friction resistance of the fluid. Combined with Equation 5.3.5 the max shear stress in the gap is,

$$\tau_{max} = \mu \frac{u_e}{D} \tag{5.3.7}$$

Fluids exhibiting this characteristic are known as Newtonian Fluids. The max Couette shear stresses for the three main capsule speeds are compiled in Table 5.2.

Table 5.2: Max Couette shear stress in suspension gap.

Fluid Speed (m/s)	$\tau_{max}(N)$	
	Min Gap	Max Gap
$u_{low} = 134.11$	15.754	6.059
$u_{mid} = 248.11$	11.505	4.425
$u_{max} = 339.75$	6.219	2.392

While Couette flow analysis may provide a good approximation for the flow behavior in the regions between the capsule and the tube wall and be acceptable for the aerodynamic analysis, it does not tell the whole story. Lubrication theory is required to fully understand the gap behavior.

5.3.4 Lubrication Theory

Lubrication theory (hydrodynamic theory) was developed to study the friction in journal bearings and learn the best methods of lubricating them [5]. The small air bearing gap of the Hyperloop is very similar to lubrication in a journal bearing so this method was applied. The assumptions made were:

1. The lubricant (air) obeys Newton’s viscous effect (Equation 5.3.6)
2. The forces due to the inertia of the lubricant are neglected
3. The lubricant is assumed to be incompressible

4. The viscosity is assumed to be constant throughout the film
5. The pressure does not vary in the axial direction
6. The tube wall and air bearing ski extend infinitely in the z direction; this means there can be no lubricant flow in the z direction
7. The film pressure is constant in the y direction and only depends on the x coordinate
8. The velocity of any particle of lubricant in the film depends only on the coordinates x and y

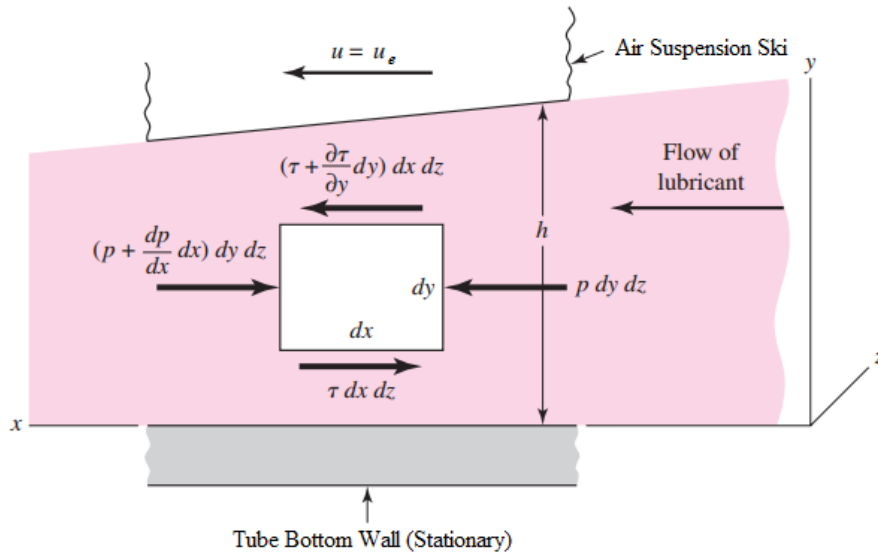


Figure 5.4: Lubrication theory schematic and force diagram.

Next, the forces acting on the sides of a lubricant element in the film of dimensions dx , dy , dz are computed (Figure 5.4). The pressure gives rise to normal forces acting on the right and left sides of the element. Shear forces act on the top and bottom sides. The force balance equation in the x-direction gives

$$\sum F_x = p dy dz - \left(p + \frac{dp}{dx} dx \right) dy dz - \tau dx dz + \left(\tau + \frac{\partial \tau}{\partial y} dy \right) dx dz = 0 \quad (5.3.8)$$

This reduces to

$$\frac{dp}{dx} = \frac{\partial \tau}{\partial y} \quad (5.3.9)$$

Substituting Equation 5.3.6 into the above equation yields

$$\frac{dp}{dx} = \mu \frac{\partial^2 u}{\partial^2 y} \quad (5.3.10)$$

Holding x constant and integrating with respect to y twice gives

$$u = \frac{1}{2\mu} \frac{dp}{dx} y^2 + C_1 y + C_2 \quad (5.3.11)$$

The constant C_1 and C_2 can be found by applying the two boundary equations

$$\text{At } y = 0, u = 0$$

$$\text{At } y = h, u = u_e$$

The final equation becomes

$$u = \frac{1}{2\mu} \frac{dp}{dx} (y^2 - hy) + \frac{u_e}{h} y \quad (5.3.12)$$

This velocity in the gap now depends on both the coordinate y and the pressure gradient $\frac{dp}{dx}$. The velocity profile is a superposition of a linear profile and a parabolic. This flow is often called Couette-Poiseuille Flow, which superimposes plate flow with pipe flow. If $\frac{dp}{dx}$ is equal to 0, then the linear Couette velocity profile will be observed. However, there will be a pressure gradient in the Hyperloop suspension air gap and a more parabolic profile will be observed. Setting $\frac{dp}{dx} = -9300$, the resulting velocity profiles can be seen in Figures 5.5 and 5.6. The parabolic nature of the velocity is very evident in the plot for the $h_{gap, max}$.

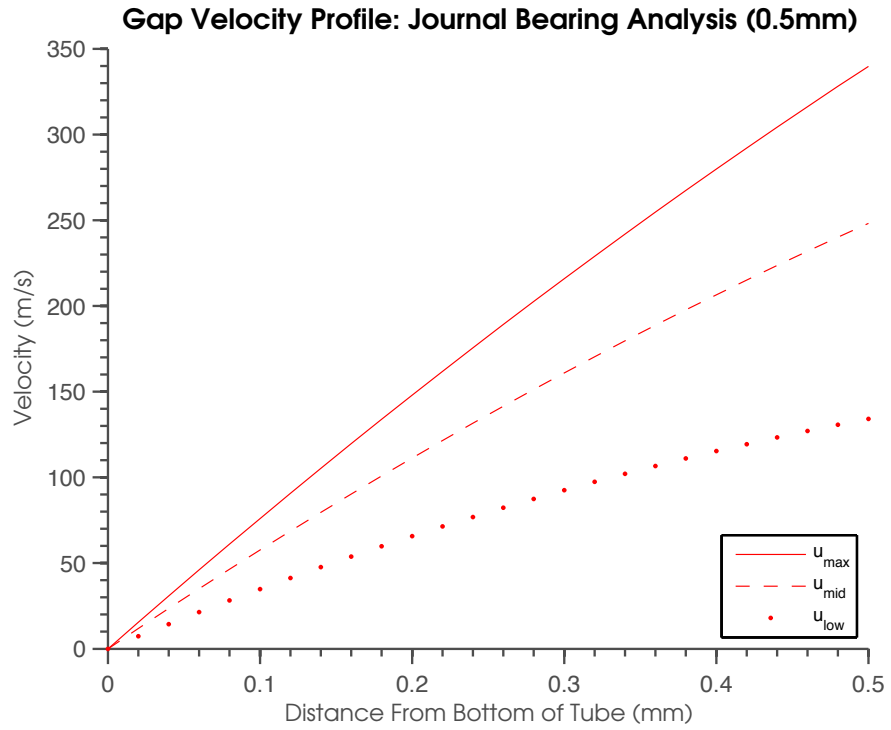


Figure 5.5: Journal bearing analysis for gap = 0.5 mm and $u_{e,max} = 339.75$ m/s, $u_{e,mid} = 248.11$ m/s, and $u_{e,low} = 134.11$ m/s.

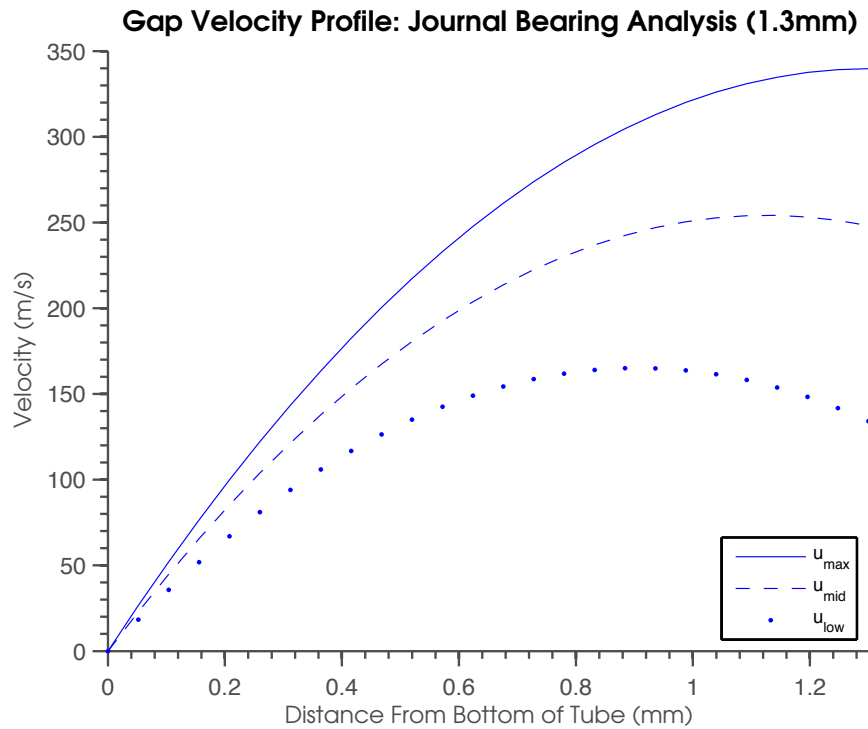


Figure 5.6: Journal bearing analysis for gap = 1.3 mm and $u_{e,max} = 339.75$ m/s, $u_{e,mid} = 248.11$ m/s, and $u_{e,low} = 134.11$ m/s.

5.3.5 Suspension Lift and Required Compressor Air Input

Mass and momentum conservation can be applied to a control volume around the air suspension ski with compressed air input enabled (Figure 5.7).

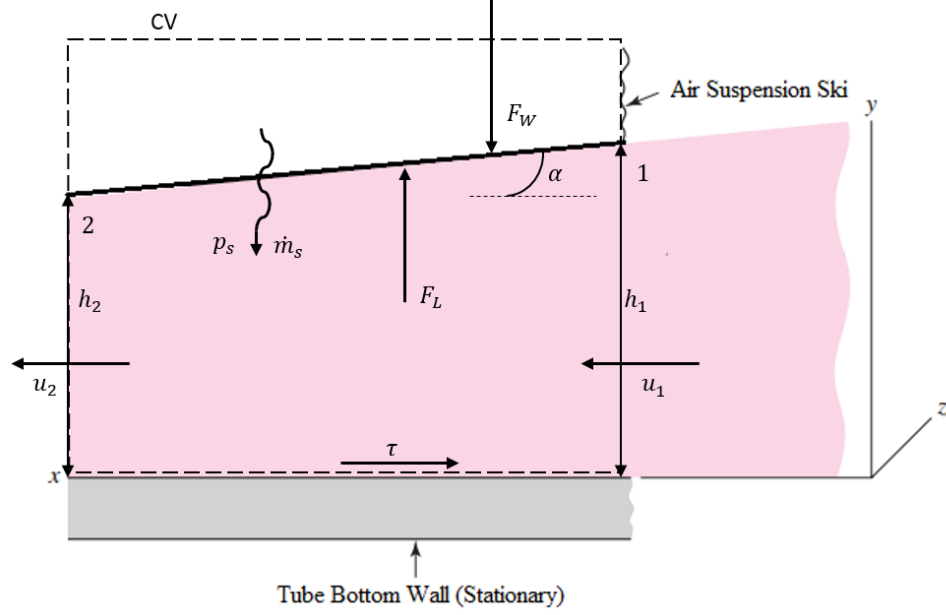


Figure 5.7: Suspension ski control volume.

Assuming a constant average density ($\bar{\rho}$), mass conservation yields the flow exit velocity at region 2

$$u_2 = \frac{1}{h_2} \left[u_1 h_1 + \frac{\dot{m}_s}{\bar{\rho} F_{W, ski}} \right] \quad (5.3.13)$$

where $u_1 = u_e$ is the inlet velocity at region 1; h_1 and h_2 are the height of the ski at region 1 and 2, respectively; \dot{m}_s is the mass flow rate of compressed air coming from the ski; and $F_{W, ski}$ is the fraction of the capsule's total weight distributed to the single ski ($F_{W, ski} = \frac{m_c g}{N_{ski}}$). Momentum conservation in the x direction gives an expression for the exit pressure at region 2

$$p_2 = \frac{1}{h_2} \left[\frac{\bar{\rho}}{2} (u_1^2 h_1 - u_2^2 h_2) + p_1 h_1 + \tau L_{ski} \cos(\alpha) \right] \quad (5.3.14)$$

where τ is the shear stress; L_{ski} is the length of suspension ski; and α is the angle of attack. Momentum conservation in the y direction provides a way to relate the lift force (F_L) to the pressure and mass flow rate from suspension system.

$$F_L = F_{W, ski} L_{ski} \cos(\alpha) (p_s + \Delta p) \quad (5.3.15)$$

where p_s is the pressure of the compressed air and $\Delta p = p_2 - p_1$.

The analysis is limited as it only deals with one ski. Regardless of the values selected for the parameters m_s and p_s the flow velocity will increase significantly by the exit to the control volume at region 2. Unless the flow is significantly compressed (much lower ρ_2 than ρ_1), the flow will become supersonic and shocks will form (the flow will also choke). This will propagate down the length of the capsule for each suspension ski. The higher the demanded mass flow rate from the air suspension, the faster the downstream velocity will be. Careful design of the shape of the suspension skis and limitations on the capsule's mass will help prevent the flow from choking in this region.

Alternatively, a conservative estimate for the lift force would assume $c_l = 2\pi\alpha$ and be computed from

$$F_{L,c} = \frac{1}{2}\rho u_e^2 A \cdot (2\pi\alpha) \quad (5.3.16)$$

For the given parameters, $F_{L,c}$ would equal 351.44 N at top speed, which is not even close to weight force the lift force must balance (4165 N). This ignores the ground effect so in reality the lift will be much higher. Cascade Theorem could be applied by modeling a series of suspension skis attached to the capsule at the 1/4-chord line and examining vortex flow. The ground effect due to the wall will create a mirroring effect of the vortices around the suspensions skis, increasing the lift coefficient. In order to balance weight force at top speed without compressed air input, the coefficient lift would need to be equal to 0.65. If the suspension ski's shape was designed like an NACA0012 airfoil, this would correspond to an angle of attack of about 6° . Now, if ground effect was considered this angle of attack would be much less. However, only a 0.5° angle of attacks seems rather small. The air suspension will need a substantial amount of compressed air input to maintain levitation.

5.3.6 Control Overview

The tube wall will not be a constant, smooth surface throughout the Hyperloop capsule's journey. The capsule will need to adapt to the changing tube landscape. A precision sensor will be needed to scan for upcoming step size changes in the tube bottom wall's contour. Investigating the control will reveal time constants, sensing distances, and maximum allowable tube changes after a given initial change. The response of the air bearing ski will be approximated by modeling a piston's movement. The "piston" chamber is the region between the tube's bottom wall and the air bearing ski with a width of $L_{ski} \cos(\alpha)$ and piston (ski) position to the wall

defined by the coordinate y (gap height).

The initial pressure in the “piston” chamber is the average between the pressure at the front and rear of the ski,

$$p_i = \frac{1}{2} \left(2p_{gap} + \frac{1}{2}\rho u_e^2 \right) \quad (5.3.17)$$

The initial position of the piston is, $y_1 = h_{gap}$.

The pressure in the chamber after a tube wall’s contour has changed can be found by assuming an isentropic process for a perfect gas, given by Equation 5.3.18. This is a valid assumption as long as the local flow is subsonic. If the local flow crosses the sonic threshold, a shock wave will form and the normal shock will process the fluid.

$$p_2(y_2) = p_1 \left(\frac{2y_1 + L_{ski} \sin(\alpha)}{2y_2 + L_{ski} \sin(\alpha)} \right)^\gamma \quad (5.3.18)$$

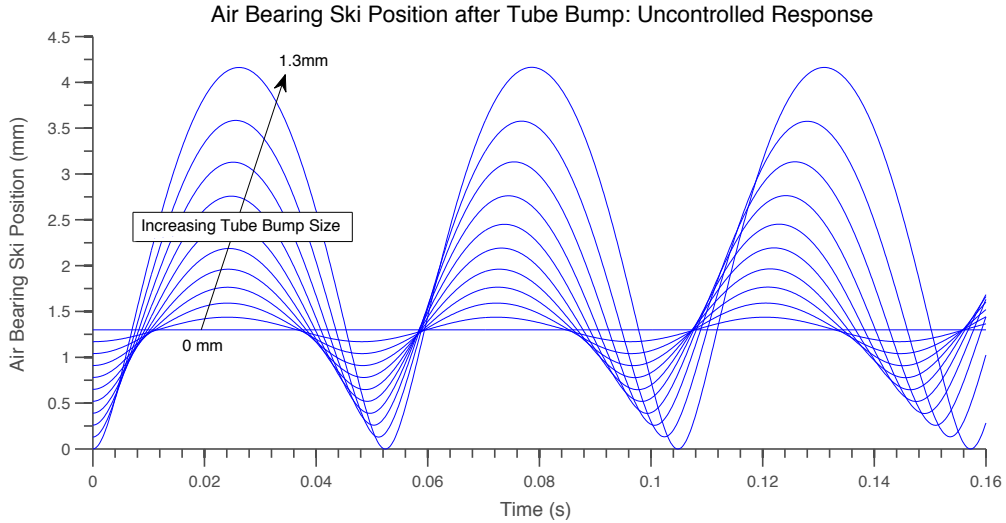


Figure 5.8: Air bearing ski position as a function of time since initial bump: uncontrolled response for gap height = 1.3mm

The restoring force of the bearing ski is given by $\Delta p \cdot A_{ski}$ and a differential equation can be solved for a given tube contour change. The zero position indicates when the rear of the ski comes into contact with tube bottom. For uncontrolled response, the oscillatory position can be seen in Figure 5.8. The larger the bump encountered, the more the ski overshoots the nominal gap height (1.3mm). For all bump heights, this overshoot of the nominal is larger than the subsequent undershoot. The period of oscillation also increases as the initial bump size increases. A suspension

control mechanism is needed to prevent the oscillations and bring the ski to rest at the nominal gap height. If a sophisticated control system is absent, the capsule may be at risk of reaching harmonic resonance in the tube. Similar to pilot-induced oscillations (PIOs) [43], sustained or uncontrollable oscillations can result (due to reduced phase margin) and lead to capsule failure.

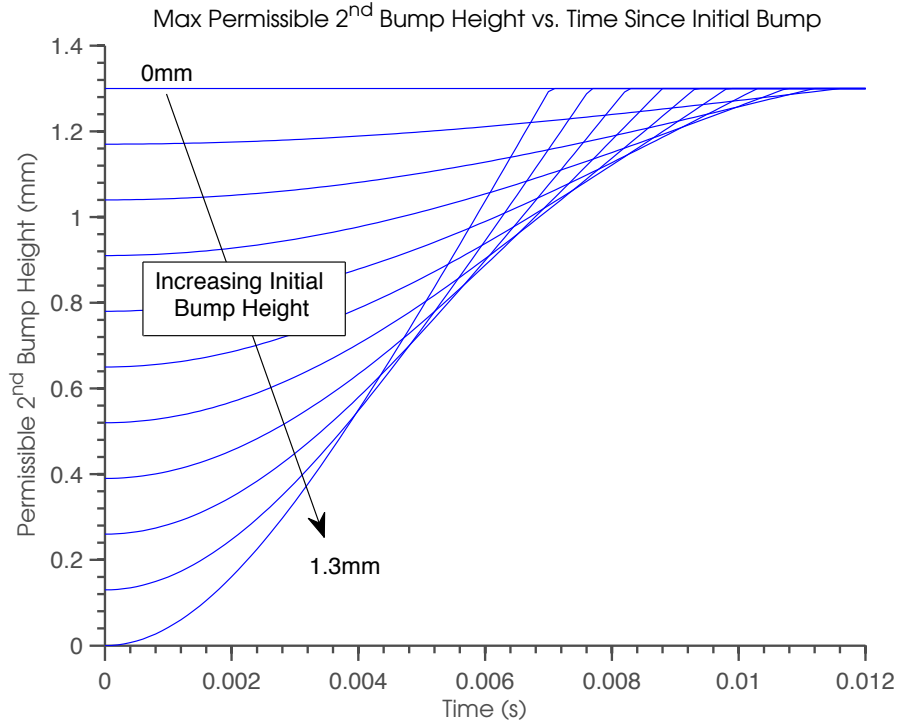


Figure 5.9: Maximum incoming tube bump height as a function of time since initial bump was encountered for gap = 1.3 mm.

How fast the ski’s position returns to nominal height is very important as it will reveal how far in advance an impermissible bump/tube change must be detected. Figures 5.9 and 5.10 show the height of a permissible second bump as functions of time and distance traveled since the initial bump, respectively. These plots focus on the position response up until it reaches nominal height. To simplify the analysis it will be assumed a control mechanism will be able to keep the ski close to the nominal height and return to equilibrium in a short amount of time after reaching the nominal height. Larger initial bumps allow smaller permissible second bumps at first, but return to nominal height faster. This effect can be observed in the figures. The necessary distance to scan in front of the vehicle will depend on how fast the measuring device can sample the ground and how fast the an actuator can respond.

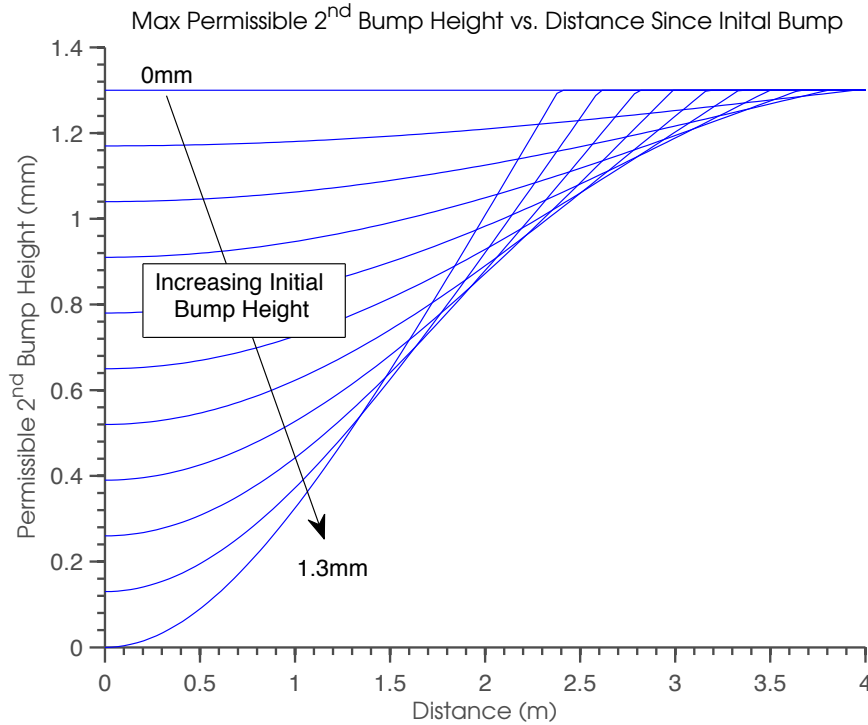


Figure 5.10: Maximum incoming tube bump height as a function of distance traveled since initial bump was encountered for gap = 1.3 mm.

In addition, since the Hyperloop capsule only floats on a thin film of air (0.5 – 1.3mm) the effect of human movement on the displacement of the capsule’s center mass is very important. Large movements can help induce harmonic resonance and lead to an effect similar to PIOs, causing failure. Figure 5.11 shows the displacement of the capsule’s center of mass downward for corresponding vertical movement of a passenger of mass 100 kg. The horizontal red lines represent the boundaries for the air gap heights. It can be seen even a small human movement upward can result in the capsule center of mass moving downward by a larger amount than either the min or max gap heights. Although the large restoring pressures may eventually return the capsule to nominal cruising height, a very robust control system with precise actuators and sensors and a fast time constant still needs to be developed in order to avoid the risk of harmonic resonance.

The center of mass equation in (5.3.19) was used to develop figure 5.11.

$$y_{disp} = \frac{m_h}{m_c} y_{move} \quad (5.3.19)$$

Chapter 6 is a case study evaluating the Hyperloop air bearing suspension system using the quarter car suspension model and applying H_∞ control synthesis.

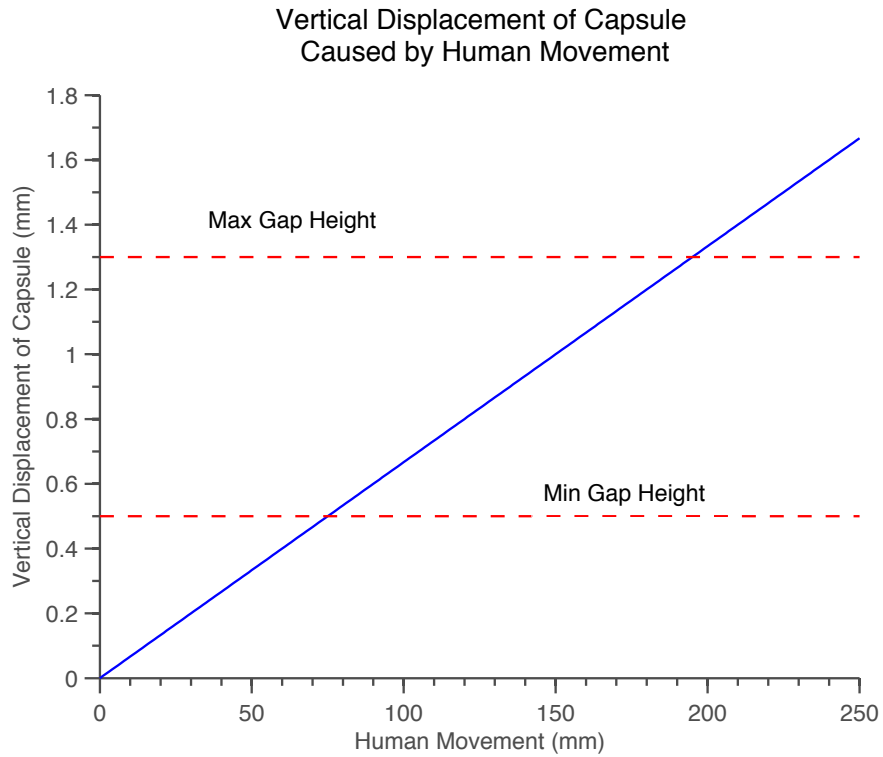


Figure 5.11: Vertical displacement of capsule center of mass due to human movement.

5.4 Maglev Cost Analysis: An Alternative Suspension Option

Maglev technology is an alternative to using an air suspension system to levitate the Hyperloop capsule. Throughout the literature costs are listed for proposed and completed maglev high speed rail systems. Some are better than others breaking down the costs to specific components, but the classification system of where expenditures are directed are quite broad, and without specific knowledge of what these categories encompass it is very challenging to isolate the costs due to the maglev system itself. After contacting several maglev experts the uniform response was no supplier has released the actual costs of maglev components, but estimates can be obtained by researching proposals and past projects. The available information on past projects is very limited because the United States has not built a maglev high speed rail system and the few nations with fully operational systems have not released documentation beyond the basic total expenditure. Proposed systems were the main source of information and it should be noted that the values presented vary and should only be

accepted with a degree of uncertainty. The largest factor contributing to variation is the literature's inconsistent cost category scheme.

The maglev technology will consist of components on both the vehicle side and the track side. These include levitation magnets, associated electronics for tasks such as air gap sensors, control software, etc., as well as guideway-mounter services (stator packs, reaction coils). These components are needed both for the suspension subsystem and lateral guidance subsystem. Propulsion is independent of these two subsystems and not considered a maglev element.

First, the vehicle side is discussed. From a capital cost breakdown document of a transrapid-style high-speed maglev vehicle provided by Laurence Blow from MaglevTransport, Inc. the maglev technology in the vehicles undercarriage comprises only 10-15% of the total cost [3]. The 2002 document lists the total capital cost per vehicle section at \$8.47 million, adjusting for inflation to 2014 this is about \$11.096 million per section. This means about \$1.1 to \$1.7 million for maglev technology per section. When considering the basic planning level a +/- 30% accuracy factor needs to be applied as well as any other contingencies. Maglev trains will typically have between 2 and 10 vehicle sections. It can be seen the maglev costs on the vehicle side are minimal and a Hyperloop system with an air suspension implementation will see costs at least this expensive. Next, the track side costs of maglev needs to be examined.

The largest costs for a maglev system arise from the civil infrastructure. To estimate these capitals cost the following proposed system and assessments were investigated: the California-Nevada Interstate Maglev Project (CNIMP), the California High Speed proposal, a 1997 assessment for a Baltimore-Newark route, and German ICE and Transrapid Routes.

In 2000, the CNIMP was estimated to cost around \$12 billion for the 269 mile (433 km) route connecting Anaheim and Las Vegas [10]. According to Figure 5.12 the guideway and infrastructure costs are 58% of the total construction cost. This amounts to \$9.615 billion for maglev related infrastructure (accounting for inflation to 2014). The details of what actually is included in the ambiguous category *guideway and infrastructure* are very unclear, but if it is assumed that only 60% of guideway and infrastructure is directly related to maglev technology and extrapolating this cost to the length of the Hyperloop track between Los Angeles and San Francisco, the capital costs for track side maglev would be \$7.6 billion. This maglev technology by itself would be more than the entire Hyperloop alpha document proposed capital costs.

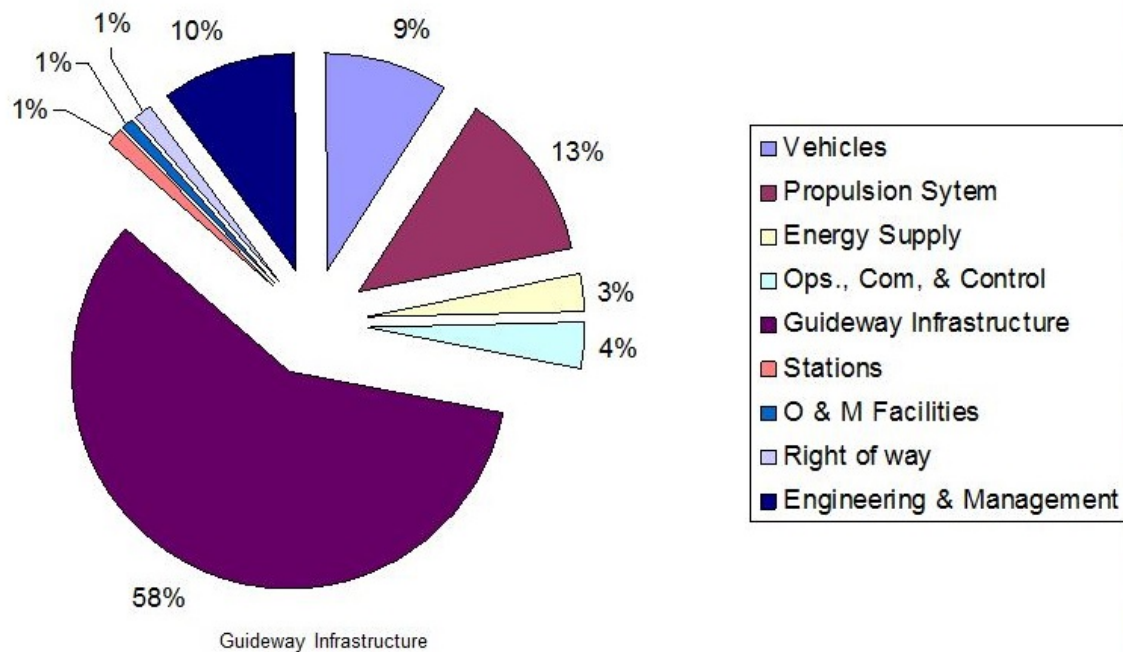


Figure 5.12: Capital construction costs for the proposed California-Nevada Interstate Maglev Project (CNIMP)[10].

The Revised 2012 Business Plan for the California High Speed Rail (CHSR) proposed between Anaheim and San Francisco paints a slightly different picture. Out of the proposed \$68.4 billion expenditure capital cost, only \$2.046 billion is estimated for the *trackwork* [8]. Again this document does not specify what comprises this category, and it may be assumed this trackwork term encompasses all the maglev components on the track side. Thus, the track side of maglev is only about 3% of the entire budget. For a proposal that appears to be more thought out, these numbers may be more accurate. Returning to the issue of category ambiguity, the report also lists capital costs for *structures* and *civil*, and these are 13.5 times that of *trackwork* (\$22.4 billion and \$5.35 billion, respectively). It is unclear whether these categories contain any essential parts specific to the maglev technology or if they are instead just overall structure costs that will be comparable to similar aspects like the Hyperloop tube and pylons.

A 1997 *Journal of Transportation Engineering* article assessed the maglev guideway cost of a potential route from Baltimore (BAL) to Newark (NWK) (264 km). The assessment considered four potential system concept designs and the cost of guideway construction cost per km ranged from \$7.6 million to \$21.1 million [42]. Accounting

for inflation and extrapolating to the Hyperloop route yields a cost range between \$6.37 and \$17.7 billion. This cost categorization does offer some more details. It mentions the estimates do not include right-of-way, propulsion, station, and other fixed facilities. The data is meant to purely estimate the construction of the guideway structure. About 20% of the estimated costs are due to labor.

The proposed guideway infrastructure costs for German Intercity-Express (ICE) and Transrapid routes range from \$30.76 to \$43.43 million (USD) per km (accounting for inflation) [51]. Based on the other costs presented, the guideway infrastructure category in this case is expected to encompass much more than maglev technology related components. Under the assumption that 50% of this category is related to maglev components, it would correspond to \$8.77 to \$12.38 billion for the Hyperloop route. These findings are compiled in Table 5.3.

Table 5.3: Maglev guideway cost assessment extrapolated to Hyperloop route

System	Low Cost (billion USD)	High Cost (billion USD)
Hyperloop Alpha Total	NA	\$6.0
CNIMP	NA	\$7.6
CHSR	\$1.82	\$2.05
BAL/NWK	\$6.37	\$17.70
German ICE	\$8.77	\$12.38

Maglev technology costs in high speed rail systems were found to vary significantly due to the ambiguity of cost categories. Some of these costs from the literature, in addition to raw maglev capital costs, may include a lot of the basic infrastructure that is needed for a Hyperloop implementing an air suspension system. It is hard to distinguish what percentage of these values would be an added cost to a Hyperloop featuring an air suspension system instead of maglev suspension. It is imperative that accurate cost estimates are available to assess the financial viability of maglev technology in the Hyperloop. More research is needed to determine if this technology should be given more serious thought. An advantage of maglev is the developed stage of the concept and its successful use in many operational systems. The air suspension system will need to be prototyped on a large scale and this process is likely to run into many challenges, adding a risk factor. The tradeoffs between using a proven system at a potentially much higher cost and spending the time/research to implement a new suspension solution on a large scale need to be considered.

*From the collections of the Princeton University Archives,
Princeton, NJ*

Statement on Copyright Restrictions

This senior thesis can only be used for education and research (among other purposes consistent with “Fair use”) as per U.S. Copyright law (text below). By accessing this file, all users agree that their use falls within fair use as defined by the copyright law. They further agree to request permission of the Princeton University Library (and pay any fees, if applicable) if they plan to publish, broadcast, or otherwise disseminate this material. This includes all forms of electronic distribution.

U.S. Copyright Law (Title 17, United States Code)

The copyright law of the United States governs the making of photocopies or other reproductions of copyrighted material. Under certain conditions specified in the law, libraries and archives are authorized to furnish a photocopy or other reproduction. One of these specified conditions is that the photocopy or other reproduction is not to be “used for any purpose other than private study, scholarship or research.” If a user makes a request for, or later uses, a photocopy or other reproduction for purposes in excess of “fair use,” that user may be liable for copyright infringement.

Inquiries should be directed to:

Princeton University Archives
Seeley G. Mudd Manuscript Library
65 Olden Street
Princeton, NJ 08540
609-258-6345
mudd@princeton.edu